Domain Wall Memory Device

34

Michael Foerster, O. Boulle, S. Esefelder, R. Mattheis, and Mathias Kläui

Contents

Abstract

Magnetic domain walls in confined geometries have attracted much interest in the last couple of years for a number of reasons. On the one hand, new physical phenomena such as current-induced domain wall motion due to the highly

M. Foerster (✉) • M. Kläui
Institute of Physics, Johannes Gutenberg-University Mainz, Mainz, Germany
e-mail: mfoerster@cells.es; klaeui@uni-mainz.de; mathias@klaeui.de

O. Boulle
Laboratoire SpinTec, CEA, Grenoble, France
e-mail: olivier.boulle@cea.fr

S. Esefelder • R. Mattheis
Leibniz Institute of Photonic Technology, Jena, Germany
e-mail: Sascha.esefelder@web.de; roland.mattheis@ipht-jena.de

Y. Xu et al. (eds.), *Handbook of Spintronics*,
DOI 10.1007/978-94-007-6892-5_48

debated nonadiabatic spin torque and novel spin–orbit torques have been investigated. On the other hand, the proposal of the racetrack memory concept as a universal data storage device has stimulated much research. In such a device, domain walls in magnetic nanowires are used as bits of information which can be shifted, e.g., to locate them at the position of a read head, without the need to move physically any material. The prospect of memory and logic devices has spurred an intense research, in particular into different materials with promising properties for domain walls and domain wall motion. The critical parameters to be optimized are mainly domain wall lateral sizes, directly governing the possible information density, and domain wall movement and pinning/depinning processes that determine access time and energy consumption. The ability to control and manipulate domain walls precisely opens up avenues to designing a range of novel and highly competitive devices.

In this chapter, a review of the properties of magnetic domain walls in nanowires and the possibilities to control and manipulate them is given. Precise control and efficient manipulation of domain walls is the prerequisite for any device. Different material classes and the resulting domain wall types are reviewed. The basic operations that are necessary for a device, i.e., nucleation, displacement, and detection of domain walls, are discussed for these material classes. Examples of devices using magnetic domain walls are briefly reviewed, including memory and logic applications. The first commercial nonvolatile multiturn sensor product that is based on magnetic domain walls and combines sensing and memory is described in more detail.

List of Abbreviations

1D, 2D, 3D	One, two, or three dimensional
3*d*	Elements from the first side group in the periodic table with 3D electron in the outer shell, from Sc to Zn, in magnetic context usually Fe, Co, Ni (Mn, Cr), and their alloys
AMR	Anisotropic magnetoresistance
ccw	Counterclockwise
CFAS	$Co_2FeAl_{0.4}Si_{0.6}$
CIDWM	Current-induced domain wall motion
CIP	Current in-plane
CMOS	Complementary metal oxide semiconductor
CPP	Current perpendicular to plane
cw	Clockwise
DC	Direct current
DMI	Dzyaloshinskii–Moriya interaction
DW	Domain wall
DWG	Domain wall generator
EHE	Extraordinary Hall effect
FTH	Fourier transform holography (with X-rays)
GMR	Giant magnetoresistance
IBM	Industrial Business Machines Corporation

IST-RAM	In-plane spin-torque random access memory
LLG	Landau–Lifshitz–Gilbert equation
LSMO	$La_{0.33}Sr_{0.67}MnO_3$
MFM	Magnetic force microscopy
MOKE	Magneto-optical Kerr effect
MR	Magnetoresistance
MRAM	Magnetic random access memory
MTJ	Magnetic tunnel junction
NEC	NEC Corporation
OOMMF	Object Oriented Micromagnetic Framework
OST-RAM	Orthogonal (perpendicular) spin-torque random access memory
PEEM	Photoemission electron microscopy
PL/FL/AL	Perpendicular magnetized layer, free layer, analyzing layer
PMA	Perpendicular magnetic anisotropy
Py	Permalloy ($Ni_{81}Fe_{19}$)
RAMAC	IBM 305 RAMAC (random access method of accounting and control), first computer with a hard disk drive
RF	Radio frequency
SEM	Scanning electron microscopy
SEMPA	Scanning electron microscopy with polarization analyzer
STO	$SrTiO_3$
STT-RAM	Spin transfer torque magnetic random access memory
STT	Spin transfer torque
STXM	Scanning transmission X-ray microscopy
SW	Spin wave
TEY	Total electron yield
TMR	Tunnel magnetoresistance
TW	Transverse domain wall
VW	Vortex domain wall
XMCD	X-ray magnetic circular dichroism
XMCD-PEEM	X-ray magnetic circular dichroism–photoemission electron microscopy

Constants and Quantities (in the order of first occurrence)	
μ	Domain wall mobility
μ_0	Vacuum permeability
A	Exchange constant
D, d	Diameter
e	Electron charge
H_{eff}	"Effective" magnetic field acting on **m**
H_k	Anisotropy field
$H_{nucleation}$, H_n	Nucleation magnetic field for domain walls
H_P	Propagation magnetic field for domain walls, pinning field

H_W	Walker breakdown field
j_c, J_c	Critical current density
K	Magnetic anisotropy constant
K_d	Magnetostatic energy difference between Bloch and Néel wall; demagnetizing energy
K_{eff}	Effective anisotropy constant
m	Magnetization vector
M_S	Saturation magnetization
$N_{X,Y,Z}$	Demagnetizing factors
P	Spin polarization
RT	Room temperature
t	Thickness
T_C	Curie temperature
u	Effective velocity
w	Width
α	Damping constant
β	Nonadiabatic
γ_0	Gyromagnetic ratio
θ	Out-of-plane spin-canting angle
λ_{ex}, Λ	Exchange length
λ_{sf}	Spin-flip length

Introduction

In the past, magnetic nanostructures have been at the heart of a multitude of devices ranging from sensing applications to data storage. Probably the best known storage device is the magnetic disk drive [1], pioneered in the 1950s by IBM with the RAMAC. Since then, storage density has seen a gigantic exponential increase. While hard drives continue to excel in the high-capacity market, they nonetheless possess disadvantages that have led to other memory concepts replacing them for certain applications, such as lower-density mobile storage. One of the key problems is the mechanical motion of the media that poses reliability questions and can lead to catastrophic failure in the case of mechanical shock. Additionally the limit of random access speed in a hard disk drive due to mechanical lag and rotation also constrains its use in some data center application. Another successful form of magnetic memory is magnetic tape, with a huge capacity but obvious limitations when it comes to random access [2]. Like the disk drive, tape drives physically move the media (tape), leading to wear. Another disadvantage that accompanies physical motion is large power consumption, which in laptops leads to a significant portion of the power being used by the hard drive. For many of the growing memory markets, in particular in mobile applications (laptops, tablets, smartphones), low power combined with a solid-

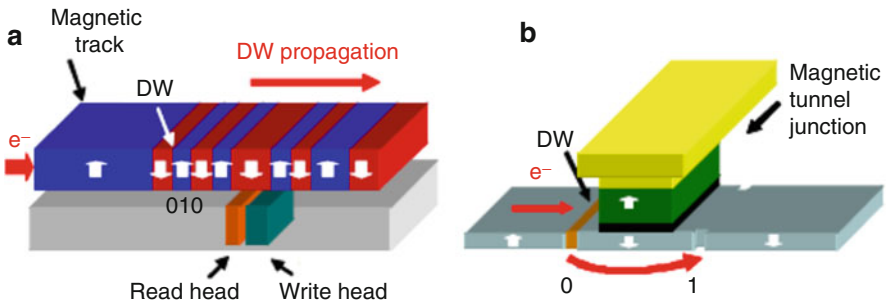

Fig. 1 (**a**) Schematic of a memory device based on a magnetic wire with domain walls. The colors and the *arrows* indicate the domain magnetization direction, which in the figure is pointing perpendicular to the nanowire. The domains with the magnetization pointing down (*red*) correspond to a logical "0," and magnetization pointing up (*blue*) corresponds to a "1." (**b**) A simplified memory based on a domain wall, which is moving between two positions thereby reversing the alignment between the magnetization in the fixed layer (*green*) and the wire below from antiparallel to parallel. Here only one bit is stored, but a simplified operation by moving the domain wall is possible without the need to "write" new domains or domain walls (From Ref. [3])

state technology is required. Different approaches have been suggested based on a range of technologies, but for magnetic data storage, a paradigm shift away from hard drives and tape is required.

One exciting approach recently proposed is based on magnetic nanowires with magnetic domains acting as the bits (Fig. 1a). The interface between 2 domains where magnetization points in opposite directions is called a magnetic domain wall, in which the spins turn by 180° and the nanoscale spin structure depends on the material and geometry. At first sight, the design looks similar to tape, but rather than shifting the media along with the data as in the case of tape, here the data is shifted within the media that stays physically fixed, leading to much faster achievable access times and, in particular, eliminating all mechanical motion.

Moreover, the device only comprises one write or read element for potentially tens to hundreds of bits, which can make it cost-effective. Furthermore, this simplifies integration with the necessary semiconductor electronics that can therefore be more compact and thus leads to higher storage densities compared to magnetic random access memory [4]. Prominent suggestions for concrete realizations of such a device are the racetrack device envisaged by S. S. P. Parkin of IBM [5, 6]; the simplified 1-bit memory pursued, for instance, by NEC (see Fig. 1b); and the shift register proposed by R. Cowburn [7]. To make the device useful for memory storage, three key tasks have to be performed; the data needs to be written, read, and selected, meaning that the bit to be read or written needs to be addressed (for instance, by moving it to the read or write element). The writing can be performed by using appropriately designed write heads, such as strip lines that generate magnetic fields by currents to reverse

the magnetization and thus "write" a bit. This can be compared to the well-established writing of bits in magnetic hard drives, but alternative approaches with better scaling such as spin-torque-induced reversal are also being studied. The reading relies on the sensing of the domains or domain walls, very similar to hard drives, so that the well-established magnetoresistive sensing, based on giant magnetoresistance (GMR) read heads [1, 8] or tunneling magnetoresistance (TMR) read heads [8], can be employed. However, it is the domain selection by motion of the domains and domain walls that requires a novel approach and is most challenging. It is essential that all domain walls can be shifted in the same direction in a controlled way while reliably maintaining their relative spacings to preserve data integrity. Thus, the dynamic behavior of geometrically confined domain walls and their motion due to applied fields and induced current pulses have become topics of growing interest in the last years due to the intricate magnetic properties present in geometrically confined ferromagnetic structures [3, 9].

Therefore, in this chapter, we will treat these three basic operations required for any magnetic domain wall-based memory device with a focus on the domain wall displacement. Since many aspects concerning control and manipulation of the domain walls are generic for any type of device based on domain walls, we give a concise but reasonably comprehensive report on the different operations that form the basis of a memory functionality – writing, addressing, and reading or, in other words, creation, motion, and detection of domain walls – and we evaluate the performance that has already been demonstrated with the prospect of a potential device in mind. We focus on domain walls in *nanowires* as the geometrical confinement allows well-defined spin structures, good control of nucleation and movement, and high information densities as desired for devices.

This chapter starts with a first part which deals with the nature of magnetic domain walls itself in static conditions. The spin structure of magnetic domain walls and their properties are reviewed for different types of materials: *conventional* in-plane magnetized 3*d* metals such as Permalloy (Py: $Ni_{81}Fe_{19}$), materials with perpendicular magnetic anisotropy (PMA) such as Co/Pt multilayers, and advanced complex materials with high spin polarization such as Heusler compounds or magnetic oxides. Secondly, different approaches for controlling the domain wall dynamics are reviewed, where the displacement due to spin transfer torque (STT) resulting from a spin current (current-induced domain wall motion, CIDWM) is emphasized as it is the most promising approach with good scaling behavior. In particular, in PMA materials having very narrow domain walls, high spin-torque efficiencies and fast domain wall velocities might be expected.

In the final section, an overview of existing and proposed devices based on magnetic domain walls is given. Examples of emerging domain wall-based devices including a field-controlled shift register and the nonvolatile multiturn sensors are discussed, the latter being already commercially available. In another commercial realization of a domain wall-based device, the bubble memory from the 1970s of the last century is in its original form not very relevant anymore today because of the low storage density.

Domain Wall Spin Structures in Magnetic Nanowires

While magnetic domain walls are a general phenomenon which occurs, e.g., in homogenous magnetic thin films and bulk samples, only using magnetic material in confined geometries like nanowires or disks allows one to generate well-defined spin structures. These spin structures, including magnetic domain walls or vortices, can be tailored by the geometry as well as the choice of material.

In general, the spin structure in confined geometries is the result of an energy minimization process (to be more precise the minimization of the appropriate thermodynamic potential, which is usually the Landau free energy) [10, 11]. In the most simple case, i.e., without any externally applied fields and for materials without effective anisotropy (e.g., polycrystalline materials), the two important energy terms are the exchange energy and the stray field energy. The material-dependent exchange energy depends on the angle between neighboring spins and is at the heart of ferromagnetism. The stray field energy is the energy related to the magnetic field created outside the magnetic structure, resulting in domain formation and the shape anisotropy of the structure. Additional contributions to the overall anisotropy energy can arise, e.g., from interfaces (for instance, in PMA Co/Pt multilayers) or from an intrinsic magnetocrystalline anisotropy in epitaxially grown materials such as Fe_3O_4 or $La_{2/3}Sr_{1/3}MnO_3$ (LSMO). Already relatively small additional contributions can have a decisive influence on the spin structure, e.g., in both of the above cases, domain walls are observed [3, 12, 13], which are very different from the ones observed in materials without magnetocrystalline or interface anisotropy.

While typically the domain wall width is determined by material parameters, in the case of soft magnetic materials with large intrinsic domain wall widths, also the geometry and in particular geometrical constrictions can play a role in determining the wall width [9]. It can range from hundreds of nanometers in soft magnetic materials down to a few nanometers in high-anisotropy PMA material. Wall widths have been previously studied for domain wall types other than head-to-head walls theoretically [14] and experimentally [9, 15], and more information on domain wall-related magnetic length scales can be also found in [16, 17].

The possible information density of a memory device is however limited, not only by this width but also by the minimum distance above which the interaction of two domain walls becomes negligible. Thus, a recent approach [18] to reduce the domain (=bit) size in a magnetic nanowire is to use a stack of two ferromagnetic layers which are coupled antiferromagnetically so that domain walls in the two layers are aligned vertically above each other. In this case the stray field produced by one domain wall is strongly reduced compared to one in a single ferromagnetic layer, which implies less interaction between neighboring domain walls and thus the possibility to place them closer to one another.

The domain wall width is also one key parameter for the interaction between domain walls and spin-polarized currents, since it governs whether the interaction occurs adiabatically (meaning that the conduction electron spins follow the magnetization direction adiabatically as they pass across the wall) or nonadiabatically

(leading to scattering of the electrons and a mistracking of the spin direction compared to the local magnetization direction in the wall).

Domain Walls in Low-Anisotropy Materials

Much of the pioneering work on confined spin structures, magnetic domain walls, and domain wall motion was done using polycrystalline 3*d* metals, e.g., Py ($Ni_{81}Fe_{19}$) [9]. In such cases there are only two relevant energy terms – the exchange energy and the stray field energy – as no significant magnetocrystalline is present. In the absence of a magnetic field, a magnetic nanowire is then mainly, i.e., apart from domain walls, magnetized along its direction due to the shape anisotropy. Qualitatively this situation means that if the exchange contribution dominates, the domain wall in a nanowire should be very wide, because then the angle between adjacent spins is small, resulting in a small exchange energy term. If the stray field energy dominates, the spins try to stay aligned parallel to the structure edge as much as possible, resulting in a narrower wall.

To go beyond these qualitative considerations, numerical calculations are necessary to ascertain the spin structures that constitute local energy minima (i.e., stable wall structures). For the case of domain walls in wires, such micromagnetic simulations [19–21] were carried out by McMichael and Donahue in 1997 [22]. Two wall spin structures were predicted to occur: vortex walls (VW, see Fig. 2a) and transverse walls (TW, see Fig. 2b). In the case of the TW, the spins rotate in the plane of the structure. To reduce the energy further, the shape of the wall is asymmetric along the vertical axis yielding a V-shaped wall (Fig. 2b). The spins in the wall can either point in the up or down direction of the image in Fig. 2b but stay always in-plane. The VW exhibits a very different spin structure with varying in- and out-of-plane components. Here the spins curl clockwise or counterclockwise around the vortex core, where the magnetization is pointing in either out-of-plane direction (Fig. 2a) [25–27]. The energies of these two wall types vary with geometry and material and can be calculated from the simulations. A "phase diagram" can be deduced where the energetically favorable wall type is determined as a function of the geometry (width, thickness). To obtain the phase boundary, which delineates the region where one wall is favored over the other, the sum of the energy differences is set to zero (both wall types have the same energy). It is found that this phase boundary for a wire of width w and thickness t has the form $w^*t \approx$ const. The constant depends on the material, which means that in a width versus thickness diagram, the phase boundary is a hyperbola below which a TW is preferred. These calculations were later refined by Nakatani and Thiaville [28]. They found, in addition to symmetric transverse walls, tilted transverse walls that constitute the energy minimum in a small range of geometries; such tilted transverse walls were actually observed experimentally [29].

A systematic experimental study of domain wall structures as a function of geometry is described, for instance, in [9]. Arrays of magnetic rings (Py, Co)

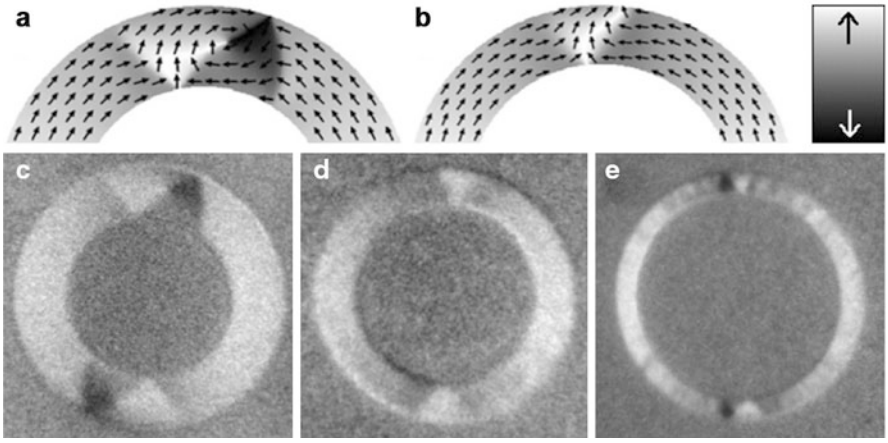

Fig. 2 (**a**), (**b**) Spin structure of a vortex (**a**) and a transverse (**b**) wall simulated using OOMMF, where *arrows* symbolize the direction and magnitude of the local in-plane magnetization. The grayscale shows the corresponding contrast for an XMCD-PEEM image with vertical beam direction. (**c**)–(**e**) XMCD-PEEM images of Permalloy rings in the onion state with different geometries corresponding to the three regimes identified in Fig. 3: (**c**) a 30 nm thick and 530 nm wide ring (outer diameter $D = 2.7$ μm) with vortex walls, (**d**) a 10 nm thick and 260 nm wide ring ($D = 1.64$ μm) showing transverse walls, and (**e**) a 3 nm thick and 730 nm wide ring ($D = 10$ μm) again with vortex walls (From Ref. [24])

were imaged using photo electron emission microscopy with X-ray circular magnetic dichroism as magnetic contrast mechanism (XMCD-PEEM), revealing the remanent domain wall spin structure after initial saturation. Some examples of observed domain walls, VW and TW, are shown in Fig. 2, together with results of micromagnetic simulations using the Object Oriented Micromagnetic Framework (OOMMF) code [30]. The experimentally determined phase diagram (wall type as a function of wire width and thickness) is shown in Fig. 3 for both Py and Co materials. While a detailed discussion of these results is given in [9], a few remarkable observations should be pointed out here: (i) the upper thickness boundary for the existence of TWs at a given width is shifted to higher values in the experiment than compared to calculations, an effect which is more pronounced in Co than in Py. This observation can be understood to arise from the fact that in the calculations global energy minima are determined, while experimentally a ring may remain in a state corresponding to a local energy minimum when decreasing the field after the initial magnetizing process. Furthermore, close to the boundary, thermally activated transitions from a TW to a VW were observed.

(ii) In the low-thickness regime of the phase diagrams shown in Fig. 3, a second phase boundary between 3 and 4 nm is found both for Permalloy and for Co. Although not expected in terms of energetics, the occurrence of VW can be explained by a spatial modulation of magnetic properties [31] such as the exchange or the saturation magnetization, which could locally allow for a stronger twisting of

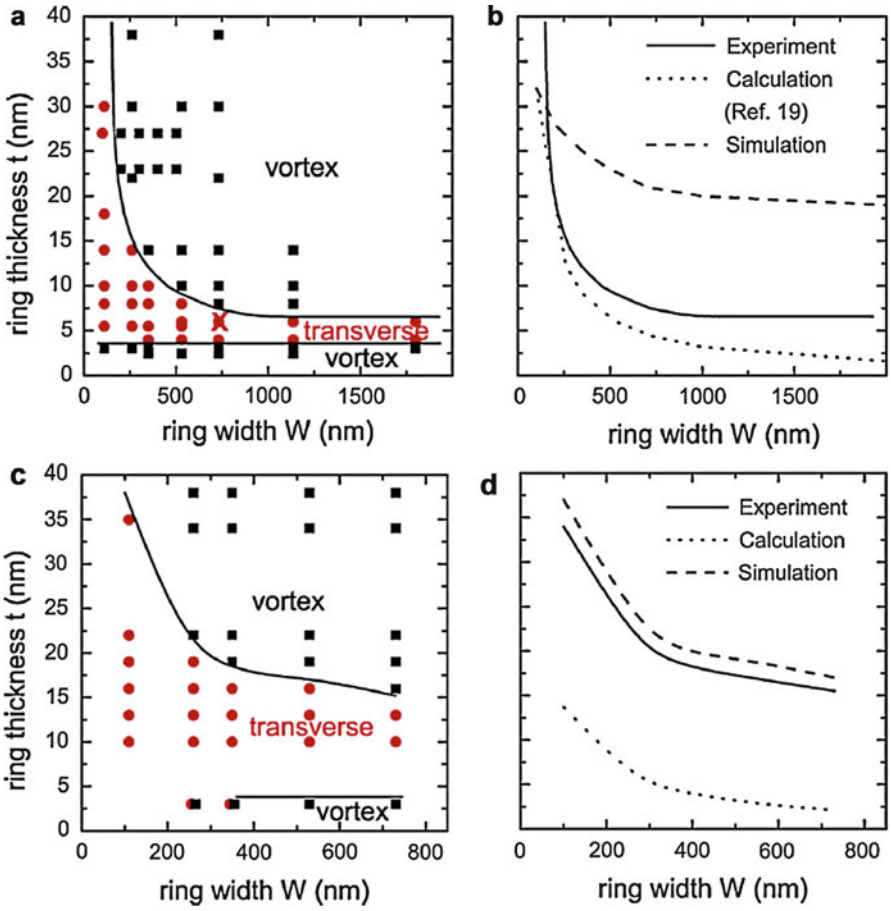

Fig. 3 (**a**, **c**) Experimental phase diagrams for head-to-head domain walls in (**a**) Permalloy and (**c**) Co rings at room temperature. *Black squares* indicate vortex walls and *red disks* transverse walls. The phase boundaries are shown as *solid lines*. (**b**, **d**) Comparison of the upper experimental phase boundary (*solid lines*) with results from calculations according to [22] (*dotted lines*) and micromagnetic simulations (*dashed lines*). The thermally activated wall transitions shown were observed for the ring geometry marked with a *red* cross in (**a**) at 730 nm width and 7 nm thickness (From Refs. [23] and [24])

adjacent spins. Also ripple domain formation, which is observed in the thinner samples investigated (Fig. 2e), can be attributed to statistical variations in the anisotropy of individual grains. The description in the context of the phase diagrams presented here is limited to a certain geometry regime. In structures that are significantly wider than $\approx$ 1 μm, other, more complicated domain wall spin structures can be found [9]. In general, in wider structures, the influence of shape anisotropy is reduced, and thus more complicated spin structures can constitute local energy minima and become observable.

Domain Walls in Advanced In-Plane Magnetized Materials

Recently domain walls in advanced materials have become a focus of research. In particular, highly spin-polarized materials, such as half-metallic oxides or Heusler compounds, are promising for spintronic applications. One important difference to the polycrystalline 3*d* metals is that these complex materials need to be grown crystallographically ordered (epitaxially or single crystalline) in order to achieve their typical, desired properties. The crystallographic order gives rise to material and growth-dependent magnetocrystalline anisotropies which influence the magnetic domain walls and their dynamics.

Fe_3O_4

Among magnetic oxides, Fe_3O_4 (magnetite) has received much interest due to its combination of high Curie temperature, multiferroic properties [32], and half-metallicity [33]. The high spin polarization lets one expect high spin transfer torque effects, which are favorable for current-induced domain wall motion in nanowires. Interestingly, for Fe_3O_4 rings, very different domain wall structures from the simple TW or VW described above were reported [13]. The Fe_3O_4 films of this study, (100)-oriented and 40–50 nm thick on MgO(100) substrates [34, 35], exhibit an in-plane fourfold anisotropy which reflects the cubic anisotropy of the bulk material, with an easy axis pointing along the [011] direction.

In Fig. 4a a high-resolution XMCD-PEEM image of a Fe_3O_4 ring structure (diameter $D = 10$ μm, nominal width $w = 1.135$ μm) which was initially magnetized by a magnetic field H along one of the magnetocrystalline hard axes (the [001] direction) is shown. The black (white) contrast reflects the horizontal component of the in-plane magnetization M. The main difference to the magnetization configurations of polycrystalline 3*d* metal rings is that here the in-plane magnetization deviates from the direction given by the shape of the structure. Instead of following the ring perimeter, the magnetization is divided into four domains. Within each of the domains, the magnetization points along one of the in-plane magnetocrystalline easy axes (the crystallographic directions are marked in the center of Fig. 4). In the neighboring segments of the ring, the magnetization vectors are perpendicular to each other, causing two straight 90° domain walls at the right and the left side of the ring (marked with A). The configuration resembles the onion state magnetic configuration observed in 3*d* metal rings [36], which is characterized by two points where the magnetic flux is not closed but instead opposing direction meet. The Fe_3O_4 ring structure contains such characteristic head-to-head and tail-to-tail domain walls, indicated by the change from black to white (and vice versa) at the top and bottom of the ring (the position of the tail-to-tail domain wall at the top is marked with B). In contrast to the transverse or vortex domain walls observed in Permalloy [9, 22], the head-to-head (tail-to-tail) domain walls in Fe_3O_4 exhibit a zigzag shape (see, e.g., the tail-to-tail domain wall marked with B).

In order to understand the remanent magnetic states observed in Fe_3O_4 rings, micromagnetic simulations of the equilibrium state at remanence were performed

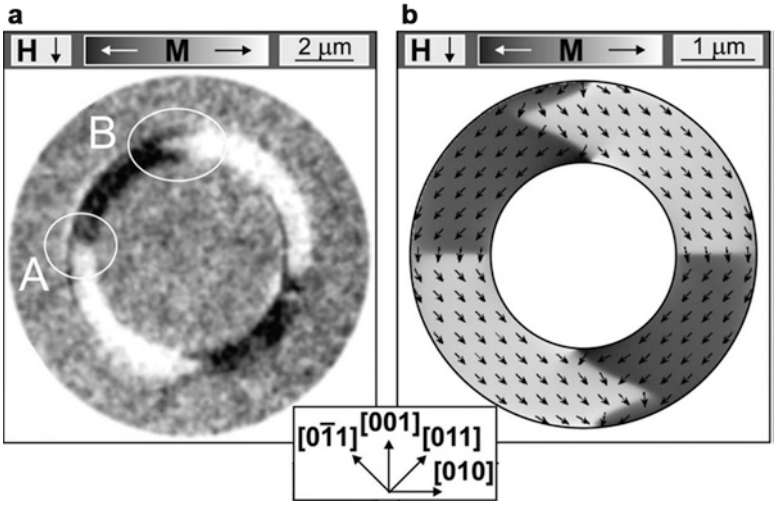

Fig. 4 (**a**) High-resolution XMCD-PEEM image of an Fe_3O_4 ring (diameter $D = 10$ µm, nominal width $w = 1.135$ µm) at zero-field. 90° domain walls are visible in the image (marked with A). A tail-to-tail zigzag domain wall (marked with B) and a head-to-head zigzag domain wall at the opposite side of the ring are also present. *Black and white* contrasts correspond to the magnetization pointing to the *left* and *right*, respectively. (**b**) Simulated magnetization orientation obtained from the micromagnetic calculation for the Fe_3O_4 ring (diameter $D = 5$ µm, $w = 1.135$ µm) in the remanent state after saturation. The samples were initially magnetized with a field H along a hard axis (the [001] direction), as indicated by the *arrow* in the *upper left corner* of each image. The in-plane crystallographic directions are marked at the *bottom* of the figure (Partly from Ref. [13])

using the OOMMF code [30]; results are shown in Fig. 4b. These simulations [13] reproduce the four-domain structure measured by XMCD-PEEM extremely well, exhibiting two 90° domain walls and two zigzag domain walls. The four-domain ring structure is a consequence of the strong fourfold in-plane magnetocrystalline anisotropy of the $Fe_3O_4(100)$ films as the magnetocrystalline anisotropy favors alignment of the magnetization along the easy axes, i.e., along the in-plane (011) crystallographic directions. The formation of the observed zigzag domain wall structure is the result of the energetic compromise between the fourfold magnetocrystalline anisotropy, the exchange, and dipolar coupling. In a ring structure, two neighboring domains meet at 90° due to the strong magnetocrystalline anisotropy, and the separating domain wall develops a characteristic zigzag shape to reduce the magnetic charge density compared with a straight wall, which would have a larger magnetic charge concentration. Thus, as the zigzag angle increases, the magnetic charge density decreases at the expense of the additional wall surface.

This strong influence of crystalline anisotropy and the relatively high resistivity are disadvantageous for a possible device based on domain wall manipulation in Fe_3O_4. For example, it would require that the nanowires were exactly aligned with the crystallographic axes to achieve a reproducible domain wall spin structure. The usual way of eliminating crystalline anisotropies in 3*d* metals by growing

polycrystalline films at low temperature cannot be followed here as epitaxial growth is needed to achieve good magnetic and transport properties.

$La_{2/3}Sr_{1/3}MnO_3$

Interestingly, $La_{2/3}Sr_{1/3}MnO_3$ (LSMO) [37], another highly spin-polarized magnetic oxide exhibits only a weak anisotropy even if grown epitaxially. The influence of the magnetocrystalline anisotropy is smaller so that spin structures can be defined by geometrical confinement as shown in [12]. For small lateral dimensions, the magnetic states fall into well-defined shape anisotropy-dominated flux closure states, with uniformly magnetized domains and sharp domain walls, similar to those found in NiFe and polycrystalline Co 3*d* metal materials [10]. This shows that, at sufficiently small dimensions, the magnetostatic energy dominates the micromagnetic configuration of the system and, in particular, that the strength of the pinning sites is smaller than the magnetostatic energy leading to geometrically confined domain walls. The fact that the epitaxial LSMO thin films are magnetically soft down to the sub-micrometer scale is not an obvious result given the presence of epitaxial strain, which tends to introduce strong pinning, and the tendency of these complex oxides to phase segregate as previously reported [38].

Ring elements of LSMO were used as prototypical structures for the study of domain walls [9]. They were found to be in the so-called onion states, corresponding to the presence of two domains in a ring, separated by two domain walls [12]. A total electron yield scanning transmission X-ray microscopy image with XMCD magnetic contrast of a 15 nm thick LSMO ring, 650 nm in width, is shown in Fig. 5a. For these particular ring dimensions, vortex domain walls (short black and white arrows) separate the two domains of the onion state (long black arrows). Figure 5b shows ring elements with widths ranging from 600 nm (II) up to 2.2 μm (III) for the 50 nm thick LSMO film; the rings favor the formation of vortex walls, although double vortex walls are also observed, as in Fig. 5b (IV) (domain wall to the right). The observed magnetic configurations can be reproduced well by micromagnetic simulations [30], showing that the spin structure in LSMO can be controlled by a suitable choice of the element geometry and that the relevant spin structures, such as well-defined domain walls, can be selectively positioned and controlled in this material, which is a key step to using this material in a device.

In conclusion, LSMO follows similar micromagnetic energetics as 3*d* ferromagnetic elements [9, 10] and has thus the advantage of not only having well-controlled spin structures but also the high spin polarization of a half-metal. Still, small remaining anisotropy energies, for instance, from the growth process, can have noticeable effects on the magnetic domain configuration [39]. Thus LSMO is a promising candidate for both, the study of fundamental domain wall phenomena in highly spin-polarized materials and for possible oxide spintronics, where robust and well-determined spin configurations are key.

The magnetoresistance of domain walls in LSMO constrictions was measured [40], and current-induced domain wall depinning in similar LSMO constriction was reported by Ruotolo et al. [41]. Although recent results [42] on domain wall motion in LSMO half rings by resistive detection at 4.2 K indicate a high spin transfer

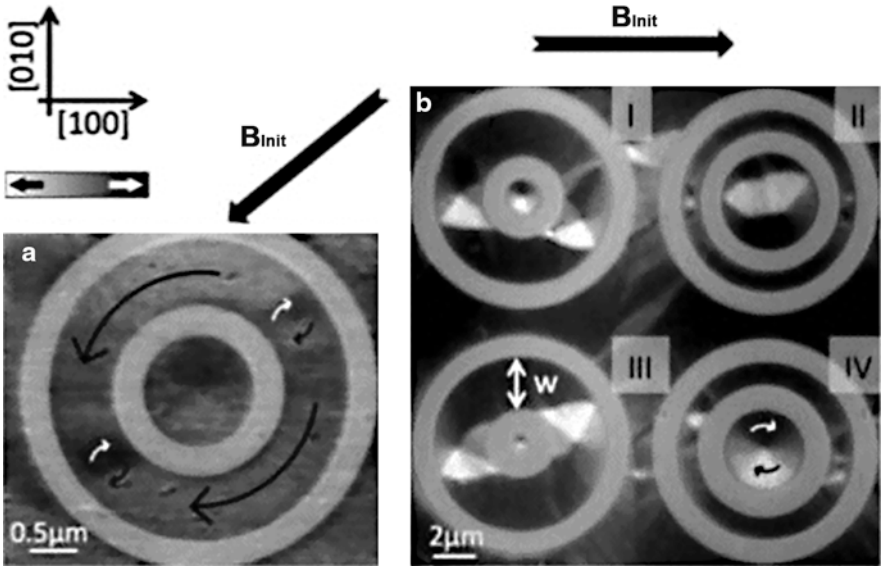

Fig. 5 Magnetic microscopy images of LSMO rings after magnetic saturation in direction of B_{init} at 300 K. (**a**) XMCD-TEY-STXM (total electron yield scanning transmission X-ray microscopy) image of a 15 nm thick LSMO/STO ring, 620 nm in width and of a 1.2 µm diameter disk in the center. An onion state is present in the ring, with vortex walls separating the two domains. The central disk is in the vortex state. (**b**) XMCD-PEEM (photoemission electron microscopy) image of 50 nm LSMO ring and disk elements. *The bold black arrows* indicate the orientation of the saturation field applied in previous imaging for (**a**) and (**b**), and *the small arrows* show the orientation of the LSMO crystallographic axes. The grayscale contrast corresponds to the horizontal magnetization as shown in the scale (Adapted from Ref. [12])

torque efficiency in LSMO, measurements performed by direct XMCD-PEEM imaging at room temperature indicate that changes in the magnetization configuration are dominated by thermal activation due to current-induced heating under these ambient conditions [43]. These heating effects, due to the relatively high resistivity and low Curie temperature of LSMO (370 K) when compared to 3*d* metals, set a limit to useable current densities and thus to practical application in a device.

Heusler Compounds

Another class of materials with high spin polarization that has been attracting significant interest for spintronics is Heusler alloys with the general formula X_2YZ, where X and Y are 3*d* metals and Z is a main group element. It was shown that Co_2MnSi is a half-metal with 100 % spin polarization even at room temperature [44] and, for instance, the compound $Co_2FeAl_{0.4}Si_{0.6}$ (CFAS) has a high spin polarization and is resistant to thermally activated changes of the magnetic domain configuration, which makes this material an interesting candidate for future applications and experiments. For CFAS grown epitaxially on Cr-buffered

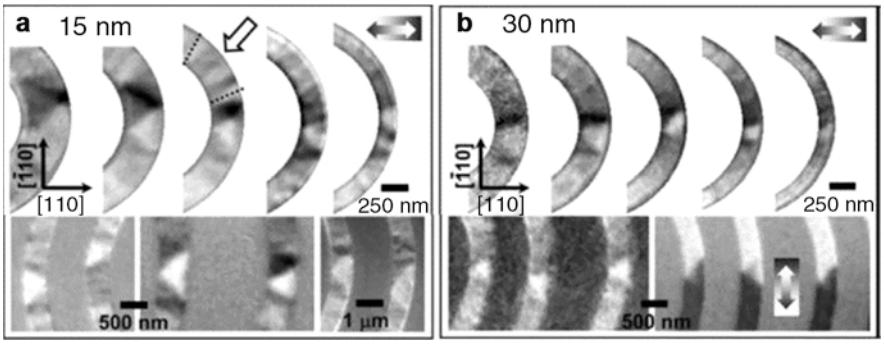

Fig. 6 XMCD-PEEM images of the spin configuration in rings and curved wires with varying width, initially magnetized along the [110] direction for (**a**) 15 nm and (**b**) 30 nm $Co_2FeAl_{0.4}Si_{0.6}$ films (300 K). The *arrow* in (**a**) points to a region in the ring element showing changes in the local transverse magnetization component that resembles ripple domains in continuous films. Note the different magnetic contrast directions in the *bottom right panel* highlighted by the grayscale bar (Partly from Ref. [45])

MgO, the control of magnetic domain configurations, for e.g., clearly defined domain wall structures, has been demonstrated [45], and further Heusler alloys have been investigated [46].

We show as an example in Fig. 6 that the magnetic configurations of CFAS ring elements after magnetic saturation consist of so-called onion states, with domain walls that divide two quasi-uniform domains in each half of the ring [48]. A strong tendency for ripple domains (which are usually associated with fluctuations in the direction of the magnetic anisotropy [49]) is found in the wire and ring elements. For narrow elements, domain wall structures are better defined, as illustrated in Fig. 6, which are explained by the stronger influence of the shape anisotropy. While transverse domain walls are dominant, vortex walls are also observed, showing that both spin configurations are stable at room temperature [9]. The domain wall structure in curved wires is found to be well defined, as shown in the bottom panels of Fig. 6. The shape anisotropy leads to head-to-head and tail-to-tail spin configurations at the wire bend, so that domain walls are formed, mostly transverse ones.

These results show that domain walls in Heusler alloys can be generated reproducibly for elements with typical widths of a few hundred nanometers, governed mostly by the shape anisotropy. The domain wall spin configuration becomes more complicated for wider elements that are more strongly affected by the magnetocrystalline anisotropy and magnetic ripple domains.

Domain Walls in Materials with Out-of-Plane Anisotropy

Soft in-plane magnetic materials such as Permalloy and LSMO have the advantage of the domain walls being less sensitive to pinning due to the large domain wall width (≈100 nm) as well as the potentially high spin polarization in some of these

materials. Experiments have however underlined serious limitations concerning the use of current-induced domain wall motion (CIDWM) in this materials. High critical current densities leading to strong Joule heating, complex domain wall structures with uncontrolled domain wall transformation induced by current injection [50, 51] that leads to unreliable and stochastic domain wall displacements [6], and domain nucleation induced by current injection [52]. These points limit the possibilities for a fundamental understanding of the spin transfer effect in magnetic domain walls but are also a serious issue for possible applications based on CIDWM.

Out-of-plane magnetized materials with a large perpendicular magnetic anisotropy (PMA) possess several advantages over soft in-plane magnetized materials: narrow domain walls typically below 10 nm with a simpler and more rigid internal Bloch/Néel domain wall structure, expected higher nonadiabaticity spin transfer torque effects due to the higher magnetization gradients and high spin–orbit coupling leading to lower critical current densities and higher domain wall velocities, and a large variety in the magnetic and transport properties of the available materials that allow one to study the dependence of spin transfer effect on these parameters. For the prospect of high-density magnetic memories based on CIDWM, these advantages combined with a small domain wall width, i.e., the small size of the magnetic bit, make these materials very attractive.

Out-of-plane magnetized materials considered for CIDWM experiments are mostly metallic thin films characterized by a strong uniaxial anisotropy oriented perpendicularly to the film plane. Two kinds of materials have been considered so far: ultrathin materials (<1 nm) where the anisotropy originates from the interface, such as in Pt/Co/Pt multilayers, and thicker (5–60 nm) materials with a magnetocrystalline anisotropy that originates in the crystalline structure of the bulk. Due to the high anisotropy, the domain wall width is very small and typically ranges between 1 and 10 nm. For ultrathin magnetic films, the thicknesses are generally smaller than the exchange length or the domain wall width so that the magnetization can be considered as being uniform across the film [53, 54] and the domain walls exhibit a nearly perfect Bloch or Néel spin structure (see Fig. 7a–b). Domain walls with nonzero internal angles (Fig. 7c) can arise, for instance, during motion of a Bloch or Néel wall so that there can be a continuous transition from one wall type to another. In a nanowire geometry, the lowest energy (i.e., equilibrium) domain wall configuration (Bloch or Néel type) depends on the geometry of the sample [3, 56], which results in different demagnetizing factors for the domain wall. For typical wire geometries considered here, Bloch walls are usually the energetically favorable spin structure.

Operation of Magnetic Domain Wall Devices

In this section we discuss the status and progress concerning domain wall nucleation, displacement, and detection in nanowires as required for a memory device. These operations correspond to basic memory functions “writing,” “addressing,”

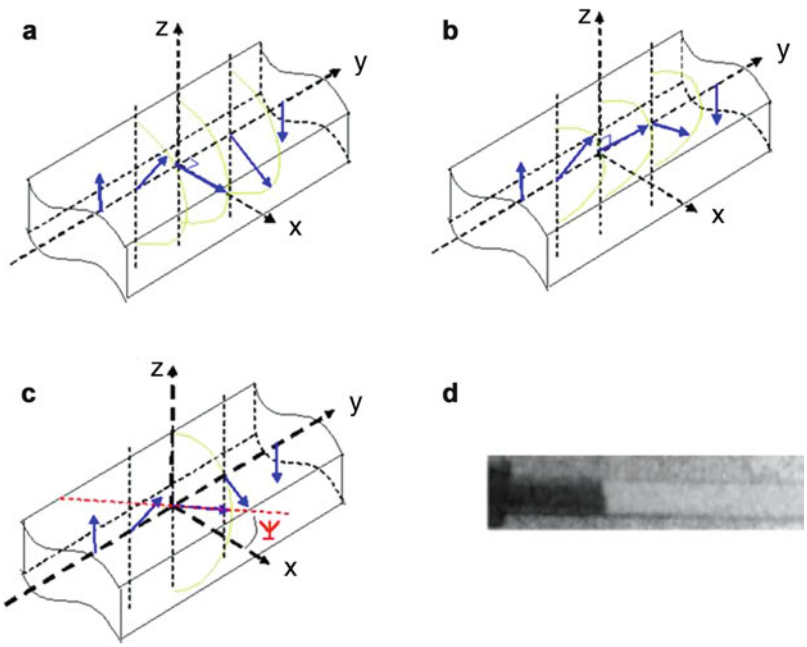

Fig. 7 (**a**–**b**) Schematic representation of a Bloch (**a**) and a Néel domain wall (**b**) in a PMA nanowire. (**c**) Domain wall with a nonzero internal angle. (**d**) XMCD-PEEM image of a domain wall in a 2 μm wide Pt/CoFeB/ Pt wire (From Ref. [3] and partly from Ref. [55])

and "reading." For a competitive device, all of these actions will need to be performed in an exact, reliable, and also fast and energy-efficient way. The one operation for which this appears most difficult at the present stage, at least in the context of the prototypical racetrack memory concept, is the addressing, which in this case is usually performed by current-induced domain wall displacement. However for other device types like shift registers and nonvolatile multiturn counters as discussed in the final section, field-controlled displacement schemes are used.

Nucleation of Magnetic Domain Walls

Similar to the displacement issue, also for the domain wall nucleation in nanowires, two main approaches exist, which either use a variable magnetic field or the spin transfer torque (STT) from an injected current. For the latter, a spin-polarized current needs to be injected into the nanowire, for instance, through a magnetic tunnel junction (MTJ) arrangement on top of it, where the nanowire acts as the free layer of the MTJ. For scaling reasons, a competitive device that uses a large number of domain walls to represent bits of information will most likely be based on spin-torque-based writing of domains and domain walls.

Global Magnetic Field and Nucleation Pads for In-Plane Materials

Previous experiments for fundamental studies of domain walls in in-plane magnetized materials mostly relied on large nucleation pads to generate a domain wall at one side of a wire structure. This approach uses a magnetic field that is sufficiently strong to reverse the magnetization in a larger pad but not strong enough to change the direction of magnetization in an attached nanowire, due to the geometry dependence of magnetic (shape) anisotropy and reversal field. Thus a domain wall at the connection point between the pad and the wire can be created by selectively reversing the magnetization of the pad only. This scheme is used, for instance, in the spiral multiturn sensors discussed in section "Non-volatile Multiturn Sensors." However, a global writing method and the requirement of big pads attached to the wires are not compatible with the needs of a potential mass storage device like the proposed racetrack memory.

Local Oersted Fields for PMA Nanowires

For materials with out-of-plane magnetization (PMA), a different approach to nucleate domain walls has to be pursued. A suitable method is to use the Oersted magnetic field created by a current in a dedicated, perpendicular ("write") wire to locally switch the magnetization of an underlying PMA nanowire, hereby creating a domain wall. The conceptual geometry is one of the simulations in Fig. 8a, where the arrangement is shown from the side. The magnetic nanowire is represented by the thick horizontal line with the perpendicular magnetization pointing either up or down. The write wire is represented by an open square, with the current flowing out of the drawing plane. The current generates a circular Oersted field around the write wire, whose direction and strength are indicated by arrows. It can be seen that at the left and right edge of the write wire, strong field components in direction of the PMA easy axis are generated by the current. This configuration is realized, for instance, in the structure shown (from top) in the magneto-optical Kerr effect (MOKE) microscopy image in Fig. 9.

This method to create domain walls has been successfully used in experiments: Ueda et al. fabricated Co/Ni multilayer magnetic wires with Au/Ti bars across as write wires. By injecting current pulses with a high current density of 1×10^{12} A/m^2 through the Au wire, they succeeded to nucleate a domain wall within the Co/Ni wire, which can be detected by a Hall bar that is also crossing the magnetic wire at close distance. In the same configuration current-induced domain wall motion can be observed as well [57]. Ohshima et al. used XMCD-PEEM to image the magnetic configuration of a Co/Ni multilayer with perpendicular magnetic anisotropy. Their work also shows that a locally created Oersted field is sufficient to nucleate single domain walls within simple nanowires [58]. Multiple creations of domain wall (injection of one domain wall after another) have been reported by Chiba et al. who also used Co/Ni multilayer wires [59].

To evaluate the scaling behavior of this approach, the local Oersted field is calculated in simulations as shown in Fig. 8. The dimensions, width and height, of the write wire (the small rectangle) are varied between 20 and 100 nm on top of a magnetic wire (long stripe) with a fixed height of 10 nm and a length of 2 μm.

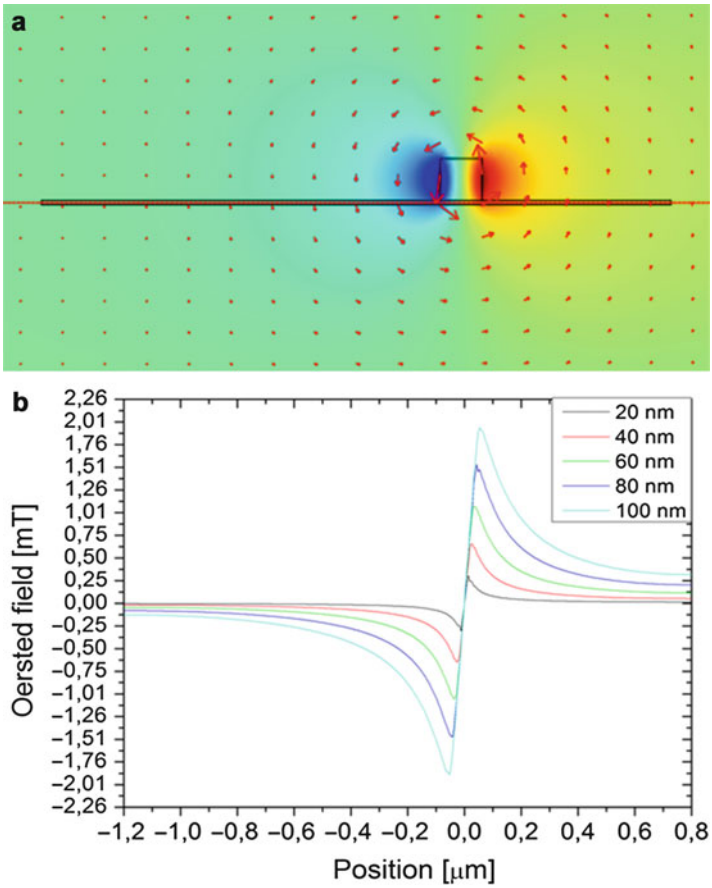

Fig. 8 (**a**) Simulation of a homogenous current density creating a circular magnetic field. The current density is perpendicular to the *small square* upon a 10 nm thin wire. The width and height of the current line (*small square*) is varied between 20 and 100 nm. (**b**) Component of the magnetic field which is perpendicular to the wire plane in (**a**) as a function of the position along the wire. The width of the current line is varied between 20 and 100 nm

A fixed current density along the write wire, i.e., perpendicular to the plane, of 1×10^{11} A/m^2 is assumed, which is a reasonable density that is compatible with reliable operation. The arrows indicate the direction and strength of the Oersted field, while the color indicates the component of the magnetic field which is perpendicular to the magnetic wire, i.e., along its PMA axis. This magnetic field component as a function of its position along the magnetic wire is shown as line scan through the middle, along the wire in Fig. 8b.

Thus, for novel low coercive out-of-plane materials, a sufficiently high magnetic field for magnetization reversal is expected in the surrounding of the current line and a localized nucleation of a single domain wall in an out-of-plane magnetized wire would be possible. Materials such as CoNi and CoFeB-based structures with

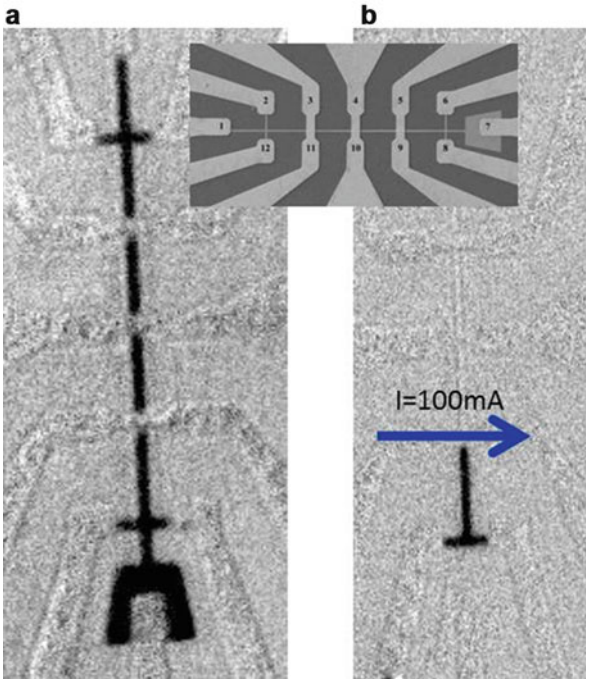

Fig. 9 (**a**) Magnetization reversal of CoFeB–MgO wires imaged by magneto-optical Kerr microscopy. As a result of a nucleation field H_n higher than the propagation field H_p, the entire wire reverses rapidly at H_n. (**b**) The use of a local Oersted field generated by a current flowing in an electrode across the wire allows the control of domain wall nucleation. Inset: SEM image of a nanowire structure (Contacts 1 and 7 in the SEM images inset) with three gold electrodes for the nucleation of domain walls through localized Oersted fields (Contacts 3 and 11, 4 and 10, and 5 and 9) and contacts for domain wall detection through the extraordinary Hall effect (2 and 12, 6 and 8) (Courtesy of D. Ravelosona)

low coercivity are suitable. In particular, CoFeB–MgO was shown to have a domain wall nucleation field of around 6 Oe only and a propagation field of around 1 Oe. Given these ultralow fields, scaling of Oersted field writing is possible even below the 90 nm design rule size.

Also combined local and global magnetic fields may be used to selectively nucleate domain walls in a defined location. The issue is that if a domain wall is created in a nanowire by a global magnetic field bigger than the so-called propagation field H_p, the domain wall instantaneously travels through the whole wire, completely reversing its magnetization as shown in Fig. 9a. Thus, to place a domain wall in a selected location, it needs to be nucleated at a magnetic field H_n smaller than the propagation field H_p. However, typically the nucleation field H_n for the creation of a domain wall in any part of the wire is bigger than H_p. But using a suitable direct current in a top electrode across the wire, it is possible to nucleate domain walls at magnetic fields lower than the propagation. One example is shown

in Fig. 9b for CoFeB–MgO structures, which have a very low typical nucleation field of 20–30 Oe, higher than the typical propagation fields ($H_p < 10$ Oe): a domain wall is here successfully placed directly under the Au cross wire that carries 100 mA current, generating a local field of around 12 Oe.

Stray Fields

Another approach for the nucleation of domain walls in selected locations is to use stray fields, i.e., interactions between domain walls. In early experiments, O'Brien et al. showed the interaction between adjacent domain walls within nanowires in close proximity [60]. Two parallel U-shaped Permalloy nanowires are used to create transverse domain walls of opposite charge. Afterwards an external field is applied to depin both domain walls. MOKE measurements revealed a larger depinning field compared to the case of single wires because of an attractive stray field interaction between the domain walls. Similar experiments have been carried out by Ahn et al. using an isolated nanobar oriented perpendicular to a nanowire [61]. Additionally a notch has been created to locally increase the pinning strength. The experiment revealed an increase or decrease in the depinning field depending on the magnetic orientation of the nanobar. Simulations of various domain wall types are used to highlight the change in the pinning potential landscape due to stray field induced by the nanobar.

The mapping of a domain wall stray field using off-axis electron holography was done by Laufenberg et al., revealing high fields of up to one Tesla at sizeable distances of the wall (100 nm) [24]. Domain wall interactions due to stray fields are also detected in a thin film experiment on Co/Cu/Ni trilayers by Kuch et al. [62]. In this experiment layer-resolved magnetic imaging (XMCD-PEEM) reveals that domain walls in the in-plane magnetized Co layer directly interact with domain walls in the out-of-plane magnetized Ni layer due to arising stray fields. The interaction can be regarded equivalent to an external field of about 250 Oe. While stray fields from adjacent domain walls or homogenously magnetized nanobars are a suitable approach to locally prepare domain walls for experiments, they limit the minimum distance of neighboring domain walls in a potential device and thus information density. As mentioned previously [63], a recent approach to reduce stray field effects between neighboring domain walls uses multilayer nanowires with coupled, opposite domain walls above each other.

Spin-Torque Reversal

However, the most promising approach for reversing the magnetization in a nanowire, i.e., writing a bit, is to use spin-torque switching because of its scalability. The switching is performed by a stack device, a nanopillar patterned on top or below the wire in the manner of a magnetic tunnel junction. The wire magnetization can be locally switched by a perpendicular current flowing from the top of the pillar into the wire, which acts as the "free layer," by the spin transfer torque (STT) [64].

Ultrafast switching by STT has been demonstrated, introducing a perpendicular polarizer in either giant magnetoresistance junctions (GMR, e.g., in Refs. [65, 66])

or in hybrid magnetic tunnel junctions(MTJ)/GMR structures [67], realizing ultrafast precessional switching on a timescale of 100 ps. Specifically, in Ref. [66], Papusoi et al. report the reproducible sub-100 ps precessional back and forth switching in a PL/FL/AL structure, where PL is a perpendicularly magnetized polarizing layer, FL is an in-plane magnetized free layer, and AL is an in-plane magnetized analyzing layer in zero effective applied field using single, unipolar current pulses. While the perpendicular polarizer can induce the precessional reversal in a subnanosecond regime, the coherence of this precessional switching was shown to be affected by thermal activation, Oersted fields, and the spin transfer influence of the analyzer as well.

In Ref. [68] Rowlands et al. report on spin-torque switching in the deep nanosecond regime by combining in-plane and perpendicular polarizers. Adding the perpendicular polarizer to a conventional spin-torque random access memory (RAM) element with an in-plane free layer and an in-plane polarizer results in significant reductions in write time and write energy when comparing orthogonal STT-RAM (or OST-RAM) structures and in-plane (IST-RAM) devices. The devices have almost identical dimensions and multilayer compositions, their main difference being the presence of the perpendicular polarizer in the OST-RAM structure, which is the key point in this study. They show that for their reference IST-RAM devices, the minimum write energy achievable is 1.25 pJ, while in the OST-RAM devices, the minimum energy is significantly smaller, down to 0.4 pJ. A further reduction in the write energy could be achieved if the MTJ formed by the perpendicular polarizer and the free layer was replaced by a GMR junction [67]. In terms of writing speed, a switching value of 0.12 ns (for a pulse amplitude of 1.58 V) is observed. Thus, for a typical multilayer structure with dimensions that are standard for an STT-RAM cell, an eightfold write time reduction and a threefold write energy reduction are demonstrated.

In Ref. [69] Amiri et al. use an in-plane CoFeB–MgO MTJ with perpendicular magnetic anisotropy in the free layer to reduce the STT switching current. They demonstrate switching at current densities of ~4 MA/cm^2 and 10 ns writing times for a reduced free layer thickness with PMA. Other reports aimed to reduce the switching current of in-plane STT devices by utilizing layered structures with transition metals (Co, Ni, and Fe) alongside nonmagnetic metals (Pt or Pd) in order to obtain the perpendicular anisotropy. However, these materials have limitations in terms of increased damping and difficulty in getting large perpendicular anisotropy in thin films ($<$2 nm) and in integrating them into MTJs with high TMR. PMA can reduce switching currents in CoFeB–MgO MTJs by counteracting the out-of-plane demagnetizing field. A breakthrough concerning CoFeB is the possibility to grow CoFeB–MgO-based magnetic tunnel junctions with PMA as demonstrated by Tohoku University together with Hitachi [70]. The perpendicular MTJs consist of Ta/CoFeB/MgO/CoFeB/Ta stacks and show a high TMR ratio of over 120 %, high thermal stability at dimensions as low as 40 nm diameter, and a low switching current of 49 μA in vertical nanopillars. This shows that this approach is also very promising to nucleate domain walls in PMA magnetic nanowires acting as the free layer of a tunnel junction.

Magnetization Reversal Using Spin Waves

Another approach to control and write the magnetization including domain walls and vortices is the creation of localized spin waves, which directly interact with the local magnetization of ferromagnetic materials. In an experiment by Kammerer et al., a rotating external magnetic field generated locally on a Permalloy disk induces spin waves, which reverses ("writes") the polarity of a prepared vortex domain wall [71].

Displacement of Magnetic Domains and Domain Walls

The crucial point for a domain wall memory device is the controlled displacement (shifting) of large numbers of domain walls. This can be done either by synchronously moving all domain walls in parallel (for instance, using spin-polarized currents as in the racetrack memory) or sequentially by locally addressing a single domain wall and then moving only this wall (for instance, using an applied field, as in the field-controlled shift register). Apart from prominent magnetic field or spin-torque-driven domain wall motion, recently other approaches have also been emerging, e.g., using local heating, spin waves, optical methods, or magnetoelastic effects through strain.

In general, the magnetization dynamics is governed by the Landau–Lifshitz–Gilbert (LLG) equation augmented by spin-torque terms. Here, the first term accounts for field effects (precession) and the second for magnetic damping, and the last two terms are accounting for effects from an injected spin-polarized current [72–74]:

$$\frac{\partial \mathbf{m}}{\partial t} = -\gamma_0 \mathbf{m} \times \mathbf{H}_{\text{eff}} + \alpha \mathbf{m} \times \frac{\partial \mathbf{m}(t)}{\partial t} - \underbrace{(\mathbf{u} \cdot \nabla)\mathbf{m}}_{\text{adiabatic}} + \underbrace{\beta \mathbf{m} \times [(\mathbf{u} \cdot \nabla)\mathbf{m}]}_{\text{non-adiabtic}}$$

(vector quantities in bold) with $\mathbf{H}_{\text{eff}}$ the effective magnetic field, γ_0 the gyromagnetic ratio, α the damping constant, and the effective spin drift velocity $\mathbf{u}$ given by $\mathbf{u} = gP\mu_B/(2eM_s)\,\mathbf{j}$. In the expression for $\mathbf{u}$, P is the spin polarization, e the electron charge, M_s the saturation magnetization, $\mathbf{j}$ the current density, and $g\mu_B$ the magnetic moment associated with the electron spin [75]. The fourth term is often called the nonadiabatic spin-torque term, but it contains not only contributions due to nonadiabatic transport but also due to spin relaxation [76]. In one theory [77], the nonadiabaticity parameter β is given by $\beta = (\lambda_{\text{ex}}/\lambda_{\text{sf}})^2$, i.e., by the ratio of the exchange length and the spin-flip length, but the theory of the nonadiabaticity is still under discussion. The reader may refer to reviews and more specialized literature [20, 21, 75, 77–80] for an in-depth discussion of these terms.

Field-Driven Domain Wall Motion

The Landau–Lifshitz–Gilbert equation [72, 74] which describes magnetization dynamics is strongly nonlinear; therefore, an analytic solution of this equation is

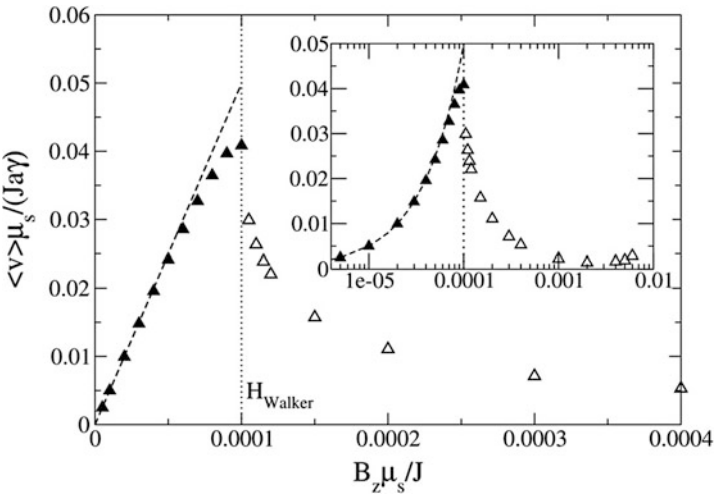

Fig. 10 Simulation of the domain wall velocity as a function of the applied field B_z for a one-dimensional spin chain (for details of the simulation and the units used, see Ref. [82]. Note that in this notation the z-axis is along the wire). The velocity increases linearly up to a critical field (Walker field). Above this field, transformations set in, which reduce the velocity. For even higher fields, the velocity increases again as seen in the inset, where a logarithmic field scale is used (From Ref. [9])

possible only for rare special cases. In order to find an analytic description of field-driven domain wall motion, Schryer and Walker [81] approximated a 180° domain wall by means of a macrospin representing the domain wall core magnetization.

In a system with an easy magnetic axis (say the x-axis in a Cartesian coordinate system), the domain wall is propagated by a field applied parallel to this axis. The domain wall dynamics are then described by two parameters in an effective 1D model: the domain wall position x and the out-of-plane angle θ, which is the canting angle of the macrospin with respect to the plane spanned by the easy x-axis and the magnetization direction of the domain wall core magnetization in the relaxed state (y-axis). (These axes are for the 1D model. While this domain core magnetization corresponds to some extent to the magnetization for a transverse wall, in a vortex wall, the two canonical conjugate variables are the x and y position of the vortex core.)

Depending on the magnitude of the applied field, one finds three regimes in the domain wall dynamics as shown in Fig. 10. For small applied fields, the domain wall velocity $v = \partial x/\partial t$ and the angle θ both increase linearly with the applied field. In this regime the domain wall mobility $\mu = \partial v/\partial H$ is positive and is given by $\mu = \frac{\Delta\gamma_0}{\alpha}$, where Δ is the domain wall width, γ_0 the gyromagnetic ratio, and α the Gilbert damping factor. At a critical field, the so-called Walker breakdown field H_w, the out-of-plane angle reaches the critical value of $\theta = \pi/4$ and the domain wall core magnetization starts to precess around the easy axis. As a consequence the mean velocity of the domain wall breaks down, leading to a negative differential

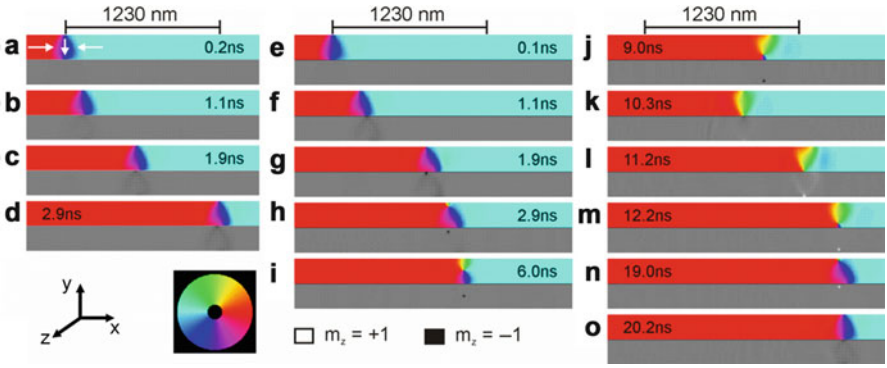

Fig. 11 Micromagnetic simulation using the MicroMagus package [96] of the dynamics of a domain wall in a 5 nm thick, 200 nm wide, and 6 μm long nanowire (cell discretization 5*5*5 nm^3). (**a–d**) Below the Walker field ($H = 0.8$ kA/m) and (**e–o**) above the Walker field ($H = 1.6$ A/m). In this case, the domain wall transforms from a transverse wall (**e**) to a vortex wall (**i**) and back to a transverse wall (**o**). The *colored panel* shows the in-plane (x–y plane) magnetization direction corresponding to the color wheel, and the *gray panels* show the out-of-plane magnetization (z-direction) with white and *black* pointing in the positive and negative z-direction, respectively

mobility μ. For even higher fields, $H >> H_w$ (see inset of Fig. 10), the mobility becomes positive again, namely, $\mu = \frac{\Delta\gamma_0}{\alpha+\alpha^{-1}}$. However, because $\alpha << 1$, the mobility above H_w is still much smaller than the mobility below the Walker field. This simple 1D model also gives an analytic solution for the critical Walker field H_w, which is proportional to the transversal anisotropy field H_k and the damping factor α: $H_w = \frac{\alpha}{2} H_k = \frac{\alpha}{2} M_s \left[N_z - N_y\right]$. $N_{(z,y)}$ are here the demagnetizing factors in z and y direction which depend on the dimensions, i.e., H_w increases with the ratio w/t of the nanowire width w and thickness t.

Simulations

A better understanding of the dynamics, especially of the Walker breakdown process for $H > H_w$, that can be obtained from analytic approaches is gained from micromagnetic simulations [19, 83–95]. For example, Fig. 11 shows the simulated motion of a transverse domain wall in a 5 nm thick and 200 nm wide nanowire using the MicroMagus package [96].

When the applied external field is smaller than the Walker field, the domain wall moves, after a short acceleration period, with a constant high velocity of $\overline{v}_{H<H_w} = 650$ m/s and a constant out-of-plane magnetization through the nanowire, as shown in Fig. 11a–d where $H = 0.8$ kA/m. Like in the 1D model, the simulations show that in this regime the out-of-plane magnetization and the domain wall velocity increase proportionally with the external field, i.e., the domain wall mobility is positive and constant.

Above the Walker breakdown, the dynamics change as shown in Fig. 11e–o for $H = 1.6$ kA/m: In the acceleration period, the out-of-plane magnetization increases

above the critical angle of $\theta = \pi/4$, and a vortex core is nucleated at the edge of the nanowire (Fig. 11g–h). This vortex core traverses the wire driven by the gyrotropic force. During this crossing the differential domain wall velocity decreases drastically and can also be negative (Fig. 11j–k), leading to a significant reduction in the mean velocity $\bar{v}_{H \gg H_w} = 70$ m/s. After the vortex core traversed the nanostripe, it is annihilated at the other edge, ending up with a reversed chirality of the transverse domain wall (compare Fig. 11e, k). This process is repeated periodically, while the edge where the vortex core is nucleated and the vortex core polarity change according to the transverse domain wall chirality.

The actual behavior above the Walker field is determined by the nanowire cross section [92]. For small cross sections, an antivortex is nucleated and crosses the nanostripe during the Walker process, while for larger cross section, a vortex is nucleated. Antivortex and vortex move in a characteristic, different manner through the nanowire: while the antivortex moves first forwards and then backwards as shown in Fig. 11e–o, the vortex trajectory is vice versa, first backwards and then forwards.

The approximation of the 1D model, treating the domain wall core magnetization as a macrospin, is only valid for small enough nanowire cross sections, i.e., when the width w and thickness t are comparable to the exchange length $= \sqrt{\frac{A}{\mu_0 M_s^2}}$, where A is the exchange constant and M_s as before the saturation magnetization. For the widely used Permalloy, this exchange length is approximately 5 nm. Thus for nanowire cross sections which are typical in terms of fabrication technology (w = 100–1,000 nm, t = 5–40 nm), micromagnetic simulations were conducted to investigate the dependence of H_w and μ on the nanowire dimensions [84]. It turned out that, contrary to the predictions of the 1D model, the critical Walker field decreases with increasing nanowire width at constant thickness. The calculated mobility increased with increasing width to thickness ratio, which is in line with the 1D model. However, the agreement is good for small dimensions only.

Micromagnetic simulations of the domain wall dynamics for fields larger than the Walker field yielded the nucleation and gyrotropic motion of vortex–antivortex pairs [87] and the formation of Bloch walls during the nanostripe reversal [95]. Further studies treated the influence of transverse in-plane fields [83, 88, 97], a unidirectional anisotropy [86], or an out-of-plane field [89], all aiming to find conditions which increase the domain wall mobility. An edge roughness added to the simulated nanostripe was found to hinder the nucleation of a vortex core during the Walker process and therefore increase the critical Walker field [94]. The influence of thermal perturbations on the domain wall dynamics was investigated by Martinez et al. [93]. They concluded that as long as the driving field is larger than the pinning field, which is due to some finite edge roughness, the changes due to thermal perturbations are negligible. The critical nucleation size of the vortex core for domain wall transformation during the Walker process was simulated in Ref. [85] and was found to be on the order of a stabilized vortex core diameter.

Experimental: Single Shot Measurements

Improvements in nanostructure fabrication and measurements techniques enabled the experimental investigation of the domain wall dynamics in nanowires. Ono et al. revealed the switching of a nanowire magnetization by means of domain wall nucleation and propagation [98, 99], and Allwood et al. measured domain wall velocities as high as 1,500 m/s [100]. An indirect experimental verification of the Walker breakdown process is the existence of a breakdown of the domain wall mean velocity, observed by Beach et al. in a single Permalloy layer by time-of-flight measurements [101]. They used the MOKE technique to detect the transit of a domain wall through the MOKE laser spot. By analyzing the transient time of the domain wall through the spot, it was possible to extract a broadening parameter, which can be explained by the existence of the Walker process [102]. A more direct measurement was performed by Hayashi et al. [103, 104], who used anisotropic magnetoresistance (AMR) measurements in order to detect changes of the domain wall configuration (domain wall type and chirality) above the Walker field H_w in single Py layers.

The direct observation of the Walker process by means of single shot measurements was performed by Glathe et al. [105] using a GMR detection technique. By choosing the reference direction of the GMR stack being parallel to the nanowire long axis, one obtains a resistance signal which depends on the magnetization component parallel to the motion of the domain wall, i.e., the signal is directly proportional to the domain wall position. Using this technique the periodic forward and backward movement, which is typical for the Walker breakdown process, was evidenced.

To improve the signal-to-noise ratio, the nanowire was contacted using a coplanar waveguide and the DC and the RF parts of the signal were separated by a Bias-T. Figure 12 shows the dependence of the RF part of the voltage from the resistance measurement for a Permalloy nanowire which is the sensor layer of a GMR stack. The periodic change between forward and backward movement is clearly visible in Fig. 12b. The inset of Fig. 12a shows the Fourier transform of the signal. The spectrum exhibits a frequency band in the range of 20–100 MHz. Note that this spectrum is different for every measurement using the same sample. Thus the Walker process is stochastic in these GMR nanowires with intrinsic edge roughness.

With the help of this GMR single shot technique, the influence of an in-plane transverse field on the Walker process was also investigated. It turned out that a transverse field decreases the Walker frequency and that a certain critical transverse field will suppress the Walker process completely [105, 106] as expected from the micromagnetic simulations [83]. The Walker process can also be suppressed by means of a superimposed oscillatory field [107] or by the use of comblike geometrical structures [115].

Further studies discovered a new type of domain wall movement [109–111] and different Walker fields in the same sample, due to the geometry of the nanowire cross section [109]. The dependencies of the Walker field H_w and the mobility μ on the dimensions of the nanostripe cross section obtained in simulations were

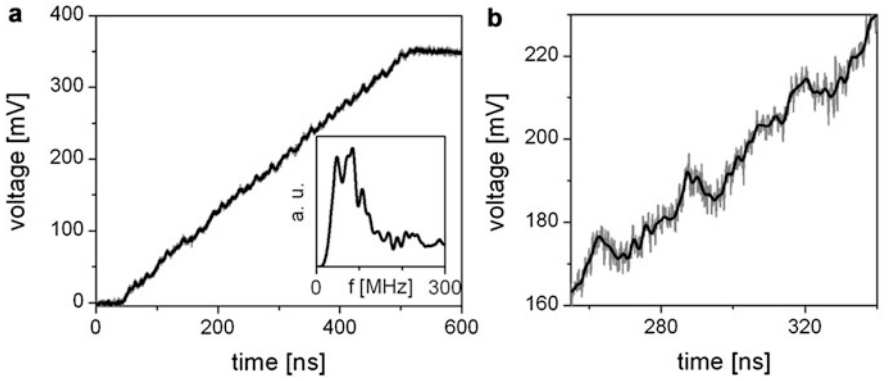

Fig. 12 (**a**) Domain wall motion in a 1 μm wide, 20 nm thick Permalloy nanowire with a nucleation pad ($H_{\text{long}} = 1.9$ kA/m, $v_{\text{mean}} = 100$ m/s). *Inset*: Frequency spectrum of the domain wall motion filtered with a Hamming filter ($N = 50$, $f_n/f_s = 0.0025$). (**b**) Magnification of the domain wall movement for a shorter period of 85 ns, corresponding to a distance of 8.5 μm. Periods of a fast-forward motion and a slow or backward motion are visible. The *gray line* represents the original data and the *black line* represents data obtained by using the Hamming filter (From Ref. [105])

confirmed experimentally [112]. Jiang et al. revealed an enhanced stochasticity around the Walker field [113]. Single shot measurements based on the TMR technique were performed by Kondou et al. [114]. They confirmed the three regimes of the domain wall dynamics and measured deviations in the linear position–time dependency. The domain wall inertia was investigated by Rhensius et al. [115] using field pulses and time-resolved photoemission electron microscopy. Finally, synchronous domain wall motion of multiple domain walls was proposed by Kim et al. using out-of-plane field pulses for in-plane magnetized wires [116].

Current-Driven Domain Wall Motion

For current-induced domain wall propagation, the expected behavior from simulations (see Fig. 13 [82]) depends strongly on the nonadiabaticity parameter β of the LLG equation above. For the purely adiabatic case ($\beta = 0$, red squares), a high critical current density j_c for propagation is observed as predicted by Thiaville [75] and Zhang [77]. Above j_c, the velocity follows a $(j^2 - j_c^2)^{1/2}$ behavior [76] and approaches the effective charge drift velocity u for large current densities. If nonadiabatic transport or spin relaxation exists ($\beta \neq 0$), the critical current density is reduced to zero for an ideal wire and the velocity increases, at first linearly, with the current density. For the case that $\beta = \alpha$ (black disks), the velocity increases always linearly, where the velocity equals u and the wall is not deformed. When $\beta \neq 0$ and $\beta \neq \alpha$ (green diamonds), the velocity scales as $\beta / \alpha * u$ up to a peak at the Walker current density. Above this value, wall transformations set in analogous to the field-induced wall motion case. Again for high current densities, the velocity approaches u. The types of wall transformations occurring for head-to-head

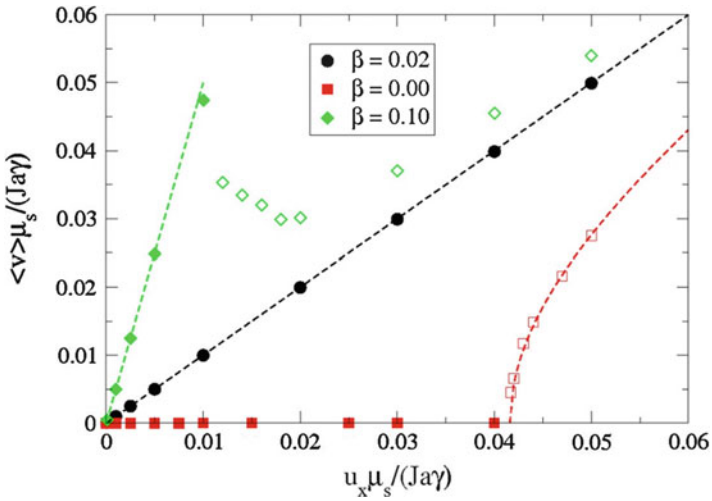

Fig. 13 Simulation of the domain wall velocity as a function of the injected current density j (for details of the simulation and the units used, see [82]). The damping constant used is $\alpha = 0.02$, and three different values of the nonadiabaticity parameter β are used: $\beta = 0$ (*red empty squares*), $\beta = 0.02 = \alpha$ (*black disks*), and $\beta = 0.1$ (*green diamonds*) (From Ref. [9])

transverse and vortex walls have been studied in detail theoretically [117] and include vortex and antivortex formation depending on the geometry and current densities used.

Experimentally, current-induced wall motion has been studied by a large number of groups (for an overview see Ref. [3, 47, 50, 103, 118–123] and references therein). Dynamic measurements of the domain wall velocity have been carried out by Hayashi et al. for the case of a dynamically generated domain wall, where velocities exceeding 100 m/s have been reported [123]. By combining current injection with magnetic fields, the velocity enhancement due to currents has been measured [122]. Starting with a domain wall at rest, slower velocities have been observed for pure current-induced wall motion [118, 119, 124]. For sufficiently high current densities, periodic wall transformations have been imaged, which points to the fact that $\beta \neq \alpha$ for the Permalloy samples used in these studies [50, 125]. Examples of experimentally observed domain wall displacements in Permalloy wires are shown in Fig. 14a for a head-to-head vortex domain wall and in Fig. 14b for a transverse domain wall. The domain walls are displaced in the electron flow direction by a short current pulse of high current density of 10^{12} A/m^2, yielding moderate averaged velocities [126].

Current-Driven Domain Wall Motion in out-of-plane magnetized material

The recent interest in out-of-plane magnetized materials has stimulated the modeling and the micromagnetic simulation of current-induced domain wall motion (CIDWM) in these materials. The main features of the domain wall dynamics in a perfect nanowire are shown to be generally well described by a simple 1D model

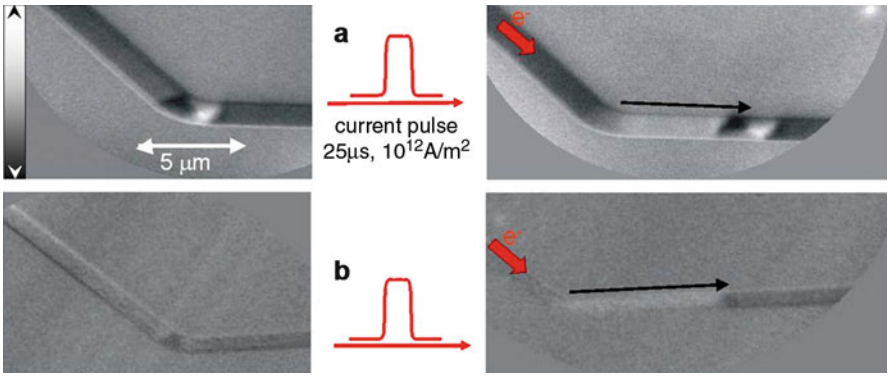

Fig. 14 Current-induced domain wall motion imaged by XMCD-PEEM. The image in (**a**) shows the displacement of a vortex wall by current injection in a 28 nm thick, 1.0 µm wide Permalloy wire with an average velocity of approximately 0.3 m/s. The grayscale bar shows the magnetic contrast direction for all the images. The image in (**b**) shows the displacement of a transverse wall in a 7.0 nm thick and 500 nm wide wire. In both cases, the wall spin structure stays the same after the displacement (Partly from Ref. [126])

due to the simple Bloch structure. However, simulations also reveal important dynamical features due to the thin domain wall structure and the different magnetic properties of these materials [26, 127–132].

Suzuki and Fukami et al. [127–129] and Jung et al. [26] studied the dependence of the critical current density on the nanowire geometry (width and thickness). Using both the 1D model and micromagnetic simulation, Jung et al. [26] showed that for narrow (typically below 100 nm) and thin (<10 nm) nanowires, the critical current density j_c does not depend on the pinning strength nor on the nonadiabaticity factor β and reaches a minimal value for a certain geometry (width, thickness) of the wire. For this critical geometry, the demagnetizing energy K_d changes sign and the domain wall switches from a Bloch to a Néel structure. The intrinsic critical current associated with the adiabatic torque is proportional to K_d and thus very low ($j_c < 10^{10}$ A/m^2). In an ideal geometry, it would vanish as the anisotropy barrier goes to zero as also in the case of round wires with shape anisotropy [133]. When the adiabatic torque controls the depinning process, the nonadiabatic spin-torque term β and extrinsic pinning effect play only little role. The geometry for minimal j_c is obtained for thick enough and very narrow wires: for a 10 nm thick film, Jung et al. [26] found the critical current density to be minimal for $w \approx 70$ nm, with the exact dimensions depending critically on the magnetic parameters.

A large number of experiments on CIDWM in out-of-plane magnetized structures were devoted to the characterization of the highly debated nonadiabatic torque. Indeed, the nonadiabaticity factor β is expected to be higher in this class of material due to the higher magnetization gradient and/or the high spin–orbit coupling [76, 134–136]. Many experiments were carried out in the presence of an external magnetic field in addition to the injected current. Indeed, the effect of the

nonadiabatic torque on the domain wall dynamics is predicted to be equivalent to an external magnetic field [75, 132, 137] so that nonadiabatic effects can be measured, for instance, by relative changes in the depinning field induced by the currents [138].

Several groups reported CIDWM at zero external magnetic field in out-of-plane magnetized materials. Despite large differences in the data provided, one can identify different groups of materials. A first group comprises of multilayers with ultrathin magnetic films and a similar order of magnitude for the efficiency ($\approx 5 \times 10^{-14}$ Tm^2/A). Due to variation in the pinning in the different films, this leads to j_c values ranging between 3 and 15×10^{11} A/m^2. Another group contains $SrRuO_3$ and TbFeCo with a much higher efficiency and a much lower critical current density in the 10^{10} A/m^2 range. Although different materials are considered, data in the first group of materials suggest an approximate scaling of the current density with the pinning strength (depinning field H_p). Several authors studied in more detail the dependence of j_c on H_p in different materials. Ravelosona et al. [139] and Li et al. [140] reported for 0.2–1 μm wide Pt/Co wires and 8 μm wide TbFeCo nanowires an approximately linear scaling of j_c with the pinning field, which is consistent with a depinning mechanism controlled by the nonadiabatic torque. However, a different scaling was reported in narrow (40–240 nm wide) (Co/Ni) wires [130, 141–143] where the critical current was found to be independent of external pinning and small (≈50 Oe) external magnetic fields. Koyama et al. [141] also studied the dependence of j_c on the wire width w ranging between 40 and 300 nm. They observe a minimum in the critical current density for a given width of the wire corresponding to the transition from a Bloch to a Néel domain wall where the domain wall demagnetizing field is minimum. This behavior is clearly consistent with an "intrinsic pinning" behavior where the depinning process is driven by the adiabatic torque in this case. Indeed, the critical current associated with the adiabatic torque can be lower than the one associated with the nonadiabatic torque for narrow wires due to the small domain wall demagnetizing field. The nonadiabatic torque thus plays a minor role in these experiments. A similar conclusion was drawn from experiments in 140 nm wide Ta/CoFeB/MgO samples [144] where the depinning current was found to be independent of the depinning field. Contrary to the case of Pt/Co/AlOx samples, the nonadiabatic torque seems to play a minor role in these structures, which may be related to the absence of Rashba coupling found in these samples.

Several authors studied the dependence of the domain wall velocity v on the current density j [45, 145–148]. As for field-induced domain wall motion, also upon increasing j (Fig. 15), one successively observes a slow creep regime where domain wall motion is controlled by wall pinning and thermal activation and a flow regime with high domain wall velocity, increasing linearly with j. In between, an intermediate regime with a higher slope $v(J)$ is observed, which may be identified as a thermally activated depinning regime.

The flow regime was observed by Moore and Miron et al. [147, 148] in Pt/Co/AlOx and Koyama et al. in (Co/Ni) nanowires [150]. In Pt/Co/AlOx nanowires, the velocity is found to increase by 120 m/s per 10^{12} A/m^2 and a maximum velocity of

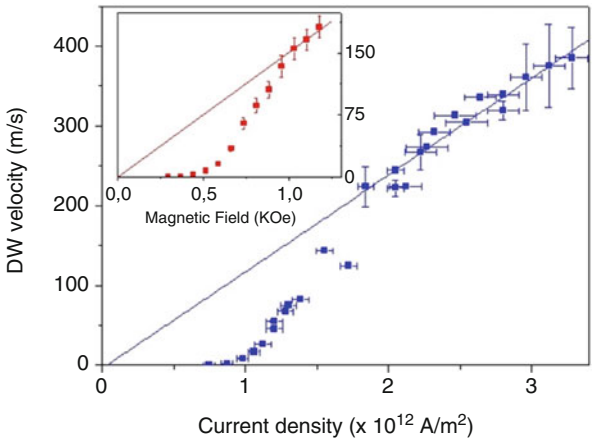

Fig. 15 Velocity of a magnetic domain wall as a function of the injected current density in a 500 nm wide Pt/Co(0.6 nm)/AlOx wire. *Inset*: Velocity of the domain wall as a function of the external magnetic field (Adapted from Ref. [149])

400 m/s is obtained for $J = 3.5 \times 10^{12}$ A/m^2 (Fig. 15). Importantly, by comparing this slope to the one measured from the field-dependent $v(H)$ curve (Fig. 15(inset)), the authors deduce a field/current equivalency identical to the one obtained from quasi-static measurements. This clearly indicates that the nonadiabatic torque is the driving force for the domain wall motion in this regime and that the domain wall is in a steady flow regime. The authors also propose that the strong transverse in-plane Rashba field identified in this structure [151] plays an important role in the motion by stabilizing the domain wall spin structure and preventing the occurrence of the Walker breakdown (the angle ψ is frozen), which in the case of PMA material would correspond to transformations between Bloch and Néel type walls. As a consequence, the domain wall stays in a high-mobility regime with $v = \beta u/\alpha$ up to very high current densities. In (Co/Ni) nanowires, Koyama et al. [150] observed that the velocity increases by about 50 m/s per 10^{12} A/m^2 and a maximum velocity of 55 m/s was reported for $j = 1.3 \times 10^{12}$ A/m^2. Interestingly, in this case, a small external applied field (up to 50 Oe) does not change the domain wall velocity and the domain wall moves in the direction opposite to the electron flow. Micromagnetic simulations show that this behavior is consistent with a precessional flow regime driven by the adiabatic torque. Fast CIDWM was also observed in TbFeCo nanowires [152] with a maximum velocity of 60 m/s obtained for a low current density of 2.5×10^{11} A/m^2 corresponding to a very high efficiency of 240 m/s per 10^{12} A/m^2.

Most authors observe CIDWM in the direction of the electron flow. However, Moore et al. [147] and Lee et al. [145] observed domain wall motion in the direction opposite to the electron flow which was proposed to be due to a negative current spin polarization or a negative β value or additional spin–orbit torques. In these studies, the nonadiabatic torque β was identified to be the main driving force on the domain wall motion. Negative β values were predicted by Garate et al. [135] in materials with high spin–orbit coupling. This result also indicates the strong dependence of nonadiabatic effects and polarization on the exact structure of the

material. Generally there is consensus now that additional may lie in additional current-induced torques due to the spin Hall effect or the Rashba effect in ultrathin multilayer with structure inversion asymmetry and/or a high atomic number nonmagnetic layer with strong spin–orbit coupling such as Pt occur [151, 153–159]. These additional torques were shown to allow for CIDWM in the direction opposite to the electron flow, and the sign of the displacement can be set by the sign of the spin–orbit torques resulting from the spin Hall effect as well as the sign of the Dzyaloshinskii–Moriya interaction (DMI) [154, 159].

These experiments have shown that the current acts on the domain wall dynamics in out-of-plane magnetized wires as a Slonczewski and a field-like torque depending on the domain wall structure, and one of them can lead to an effective large nonadiabaticity that however results from spin–orbit interaction effects. From the current-field equivalence, values of the nonadiabaticity are found that are much larger than for in-plane magnetized wires.

Although usually narrow Bloch walls are favored in PMA nanowires due to the magnetostatics; however, Néel walls can be stabilized in case of strong DMI in multilayers with inversion asymmetry, and the spin–orbit torques act on these efficiently [157, 159]. Due to the strong pinning in these materials, initially most experiments were carried out in the thermally activated regime and actually probed the deformation of the pinning barrier by current, but alter it was found that in the viscous flow propagation regime very high domain wall velocities can be obtained (up to 400 m/s) [149]. The origin of this high velocity is hotly debated and is probably due to the high spin–orbit coupling in these material stacks. An explanation based on the Rashba transverse field alone seems to be not generally accepted, and an alternative explanation based on a combination of the spin Hall effect [155, 159] and Rashba interaction [153, 154] has been put forward theoretically [160].

The high spin-torque efficiencies in out-of-plane magnetized materials make them promising candidates for domain wall memory devices. However, although very low critical current densities (down to the 5×10^{10} A/m^2) have been obtained, fast domain wall motion was so far only observed at very high current densities ($> 10^{11}$ A/m^2). A first challenge is thus to decrease the current density while maintaining fast motion. This may be achieved by decreasing the intrinsic pinning in the materials but also by engineering new materials with higher spin transfer efficiency and lower damping, for e.g., by playing with the spin–orbit coupling. The use of a transverse magnetic field to pin the dynamical domain wall structure [97, 149, 161, 162] and prevent the occurrence of the Walker breakdown (with associated lower mobility) also seems promising. Furthermore, this approach provides an interesting way of controlling the domain wall structure with the current polarity which may be exploited in devices [149, 162].

An alternative route is the injection of a spin-polarized current perpendicularly to the nanowire plane [163–166], where high domain wall velocities have been predicted at very low perpendicular current (up to 80 m/s down for 10 μA) [164]. This was confirmed experimentally by Boone et al. [165] who measured a domain wall velocity up to 800 m/s at very low critical current density

(9×10^{10} A/m^2) in Permalloy nanowires excited by spin-polarized current applied perpendicular to the nanowire. Similarly, Chanthbouala et al. [167] reported CIDWM induced by a vertical current in magnetic tunnel junctions for a low current density of about 3×10^{10} A/m^2.

A remaining issue is that the high intrinsic pinning in out-of-plane magnetized materials can lead to unreliable displacements [147] and further complicates the exact control of the domain wall position in a data track, requiring artificial pinning sites. Another challenge is thus to decrease the intrinsic pinning of the materials and to engineer efficient desired pinning sites, for instance, geometrical constrictions, to control the domain wall position on the nm scale with a high enough pinning energy compared to the intrinsic one. A possible way to reduce intrinsic pinning may be found by the use of softer compositions based on amorphous materials [55, 144, 168] or epitaxial out-of-plane magnetized materials [169].

Temperature-Assisted Domain Wall Motion

Domain wall motion may be assisted by local variations in temperature. Apart from the direct influence on local material parameters (e.g., coercivity) due to heating, an intrinsic interaction between thermally excited magnonic spin currents and domain walls was predicted [170]. This effect, which like the spin Seebeck effect belongs to the new field of spin caloritronics, is predicted to arise in wires with thermal gradients and is due to conservation of angular momentum. The domain wall is expected to move into the hotter region to compensate for the effective flow of spin angular momentum from magnons which are moving from the hotter to the colder region. Hinzke and Nowak [170] have shown that, at least for a low enough damping constant, the thermal gradient acts like an effective field, and they calculated domain position and velocity (Fig. 16) that show the same generic behavior as for field-driven motion in Fig. 10.

Indeed, Franken et al. [171] and Möhrke et al. [172] have shown that the domain wall pinning potential in a nanowire can be modified by local heating with a laser. A schematic of the experiment is shown in Fig. 17a; it consists of 1.5 μm wide, 20 nm thick Permalloy nanowires (doped with 2 % Ho) and a focused MOKE magnetometer. The nanowires have a zigzag geometry for controlled nucleation of domain walls at a bend in the wire. The magnetization is probed 3.5 μm away from the bend using the focused, time-resolved MOKE. While an external magnetic field is ramped up, the domain wall position is monitored by the MOKE signal; a typical trace is shown in Fig. 17b. One observes that the domain wall is depinned from the bend (signal level L_1) at field B_1 and moves into the laser spot where it is pinned first (signal level L_2) before the center of the laser spot until a field B_2 and a second time (signal level L_3) after crossing the center where it is depinned at a field B_3.

Interestingly, the pinning strength of the different sites exhibits a different dependence on the laser power. While the depinning field from the bend, B_1, does not change up to 14 mW laser power, the other two depinning fields are found to depend on the laser power used as shown in Fig. 18. The depinning field from the first pinning site, B_2, decreases from 8.2 G to 7.7 G, while the depinning

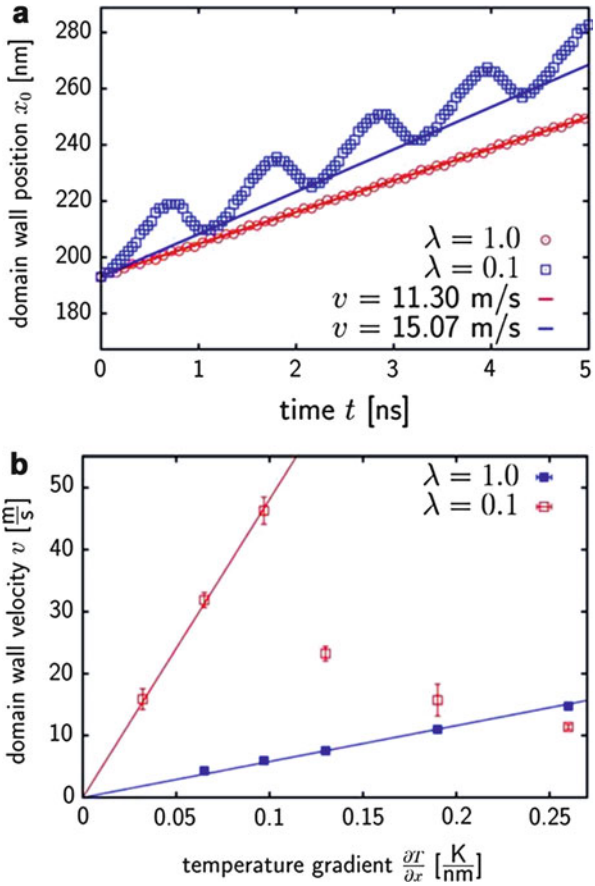

Fig. 16 Predicted domain wall motion due to interaction with thermal magnonic spin currents. (**a**) Domain wall position versus time for a temperature gradient of 0.19 K/nm and (**b**) domain wall velocity versus temperature gradient for two different damping constants λ (From Ref. [170])

field from the second pinning site, B_3, increases from 9.7 G to 10.3 G . When returning to a lower laser power, the depinning fields are found to return to the same value as before (given by the open symbols in Fig. 18). Furthermore, scanning electron microscopy images taken before and after the measurement do not show any changes of the structure. Only at laser powers exceeding the threshold $W_T =$ 15 mW, irreversible changes of the pinning behavior were found.

Estimations of the thermal gradient in the wire based on resistance measurements resulted in a very local heating of ~ 100 K, still far below T_C of Py (850 K). From this value for the temperature gradient and following the calculation of Uchida et al., a spin current of 8* 10^7 A/m^2 is expected [173], which is much lower than the order of 10^{12} A/m^2 [123], which is typically needed to move domain walls in such Py wires. Therefore, it seems unlikely that the influence of thermal spin currents is the only reason for the enhanced pinning strength caused by the laser illumination. However, the experiment shows a clear connection between laser-induced heating and pinning of domain walls, in a sense that an attractive

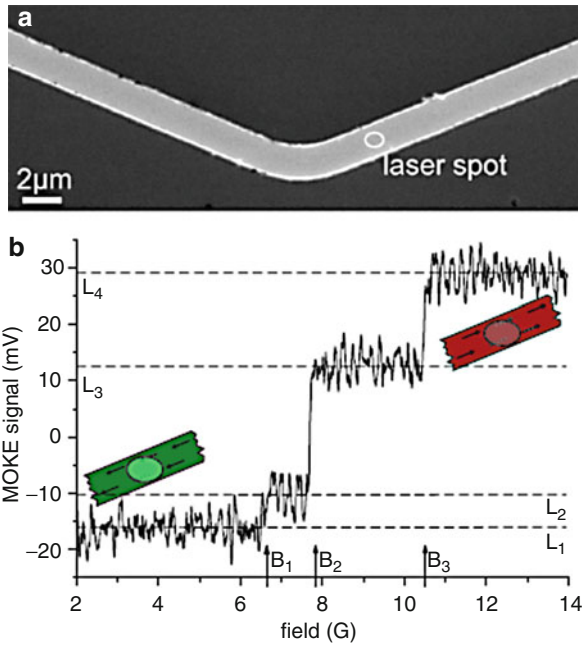

Fig. 17 (**a**) Scanning electron microscope (SEM) picture of the central part of a Permalloy wire. The position of the MOKE laser spot is shown schematically by a *white circle*. (**b**) Typical MOKE trace of a domain wall arriving at the laser spot position (B_1), where it is pinned. It is depinned from this first site at a higher field (B_2) and then pinned again at a second site, from where it is depinned at the field B_3. The laser power is 14 mW. The data is not centered around a zero MOKE signal due to an offset in the detection, which is of no importance for the measurement (From Ref. [172])

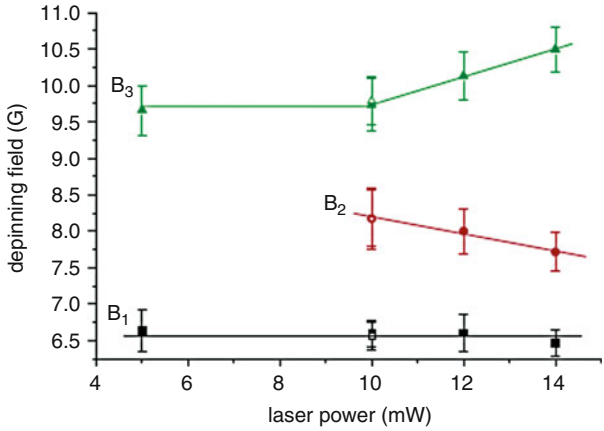

Fig. 18 The arrival field B_1 (*black squares*), which is a measure for the depinning field from the bend, and the depinning fields from the two pinning sites, B_2 and B_3, in the laser spot region (*red circles* and *green triangles*). The error bars indicate the standard deviation of 50 individual events taken for the average shown. While the depinning field of the first pinning site within the spot B_2 is decreasing the other one, B_3 is increasing with increasing laser power. The *open symbols* refer to a control measurement, which was performed after the last measurement at 14 mW. The *lines* are guides to the eye (From Ref. [172])

potential for domain walls is created by laser irradiation. This method holds promise for a way to manipulate domain walls, where a specific pinning potential can be flexibly introduced at any position along the wire and can be removed at will. Finally such domain wall motion by thermal gradients has also been observed in an insulator showing that the effect is not related to charge currents due to thermoelectric effects [174].

Alternative Approaches

In addition to the approaches presented above, further schemes have been devised to induce magnetic domain wall motion. Inhomogeneous magnetic fields transverse to the wire have been proposed [175, 176], where the energy of the transverse component of the magnetization in the wall changes with the position. This is due to the inhomogeneity of the field so that the walls are pulled toward a position where the field lowers their energy. However, due to the need for the generation of inhomogeneous fields, the experimental realization appears rather challenging.

Another possibility is to employ pure diffusive spin currents. In this case, a nonlocal spin valve geometry is used [177–180] to generate a pure spin current. When this spin current is absorbed by a ferromagnet, a change in the magnetization of the ferromagnet is possible, as seen in the reversal of a small dot [178, 181]. Domain wall nucleation has also been assisted by spin currents [182], and also wall displacement due to spin current absorption has been observed [183]. While this approach is very exciting from a fundamental physics perspective, several problems may be encountered if a large-scale realization is sought. Generating spin currents is not straightforward and the magnitude of the spin accumulation due to the spin current is mostly small due to the limited spin injection efficiency and the finite diffusion length (even though novel materials [184] might provide longer spin diffusion lengths).

The interaction of magnetic domain walls in nanowires with propagating spin waves has been treated in numerical simulations [185–187]. It is predicted that, for instance, a transverse domain wall can be moved by propagating spin waves, where the details of the interaction depend not only on the propagating spin wave frequency but also on the collective vibrations of the spin structure in the nanowires. See Fig. 19 for calculated velocities of a transversal domain wall as function of spin wave frequency [187].

Magnetization reversal by optical techniques has been demonstrated [188], and it might be possible to displace domains and domain walls by carefully designing excitations of the magnetization with a laser. Another approach that has been proposed recently is to exploit changes in the local domain wall pinning potential due to strain induced by a piezoelectric substrate [189]. Experimentally, domain wall displacement by uniaxial in-plane strain has been demonstrated in Ni rings, showing a full 90° rotation of the domain wall position [190], and domain wall deformation has also been shown [191].

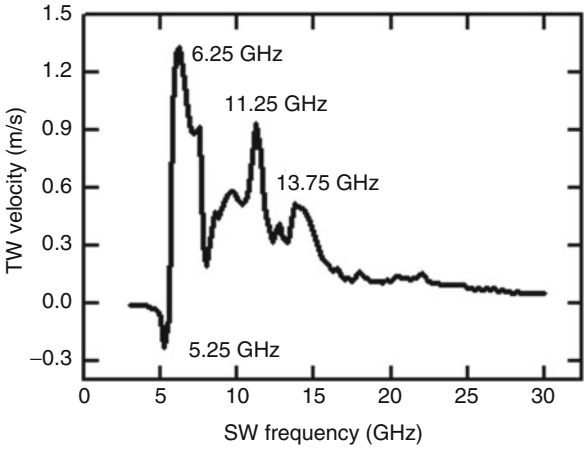

Fig. 19 Calculated transversal wall velocity as a function of spin wave (SW) frequency in a nanowire. For simulation details refer to Refs. [187] from [187]

Magnetic Domain Wall Detection ("Reading")

Direct imaging of magnetic domains and domain walls by magnetic microscopy techniques like MOKE, magnetic force microscopy (MFM), spin-polarized scanning electron microscopy (SEMPA), or synchrotron-based imaging techniques using XMCD contrast is extremely useful for scientific investigations and also allows one to resolve internal domain wall spin structures. However, obviously the readout of a potential device will have to be performed with a far more simple technique, e.g., electrical techniques that are sensitive to the presence of a domain wall by detecting changes in the magnetization. Anisotropic magnetoresistance (AMR), giant magnetoresistance (GMR) or tunneling magnetoresistance effects (TMR), and the extraordinary Hall effect (EHE) have been used to detect domain walls. For this chapter we will restrict ourselves to a short overview of the electrical readout schemes, and, since these are widely researched and mostly well established, we will not discuss these in great detail. Instead the reader is referred to the corresponding sections and chapters of this handbook. In many aspects, domain wall memory devices can profit from established sensor technology, e.g., used in hard disk drives or magnetic RAM (MRAM).

With the help of suitably placed electrodes, the presence or the position of a domain wall can be sensed by a number of different schemes. Which of these electrical sensing schemes is most convenient, depends on the material involved and other, technical considerations including signal strength, the electronic complexity of the readout circuit and integration. For systems with sizeable AMR effect [143, 190], the presence of a 180° head-to-head domain wall in a nanowire can be deduced from the in-plane resistance. The domain wall (vortex and transverse wall) includes some area where the local magnetization is not parallel to the current as it is in the rest of the nanowire, giving rise to an AMR signal. Additionally, the domain wall itself may contribute to the wire total resistance when significant

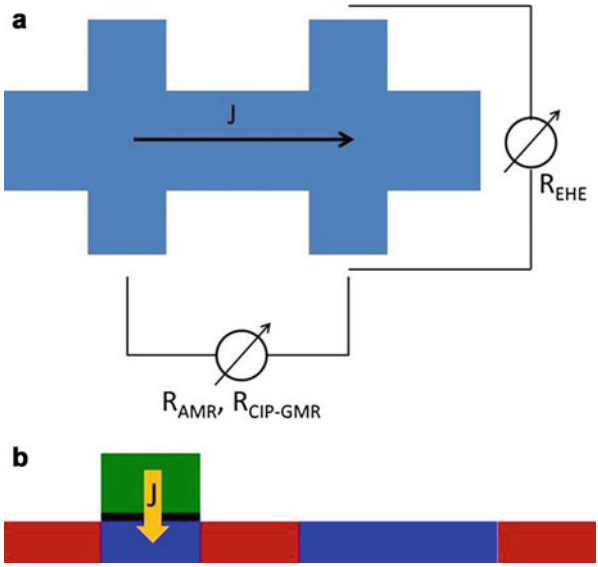

Fig. 20 (**a**) *Top view*: schematic for planar (CIP) measurement scheme for anisotropic magnetoresistance (AMR), current in-plane giant magnetoresistance (CIP-GMR), and extraordinary Hall effect (EHE). (**b**) *Side view*: nanowire with magnetic domains and nanopillar on top comprising a GMR or TMR spin valve structure. In both schematics, the direction of the injected current is shown by J

electron scattering occurs at the wall. In a similar way, multiturn sensors as discussed in section "Non-volatile Multiturn Sensors" use the current in-plane (CIP) GMR effect, measuring the resistance of a GMR stack along the wire. Another planar detection scheme which can be used with CIP geometry (Fig. 20a) is based on Hall effect measurements, which are sensitive to the magnetization perpendicular to the current flow. Thus it can be used to distinguish up and down domains in PMA material.

Techniques using current flowing perpendicular to the plane (CPP) can be GMR and TMR spin valve sensors. The wire then acts as a magnetic free layer, while a spacer/barrier layer and a second magnetic reference layer (pinned layer) are located as nanopillar on top of it (Fig. 20b). For a racetrack memory or a shift register, as well as MRAM, CPP spin valve sensors are favored, with the spin valve most likely consisting of a TMR element with MgO barrier. These sensors show big TMR signals and are CMOS compatible. If PMA materials are to be used for the faster domain wall velocities that can be achieved with them, the MTJ layout needs to include a reference magnetic layer which also has a perpendicular magnetization. Such sensors have been realized, for example, in [70].

Domain Wall Memory Devices

Magnetic Domain Wall Memory Devices

The racetrack memory device is the most prominent magnetic domain wall memory device today. It is also shown in the introduction to this chapter (see Fig.1a), and its basic concept is to use magnetic domain walls in nanowires

to store information. Bits of information are written by creating two domain walls and read back by a magnetoresistive read head, detecting the domain wall. A key ingredient is the synchronous shifting of all domain walls in one wire in either direction due to the spin transfer torque of a current passing through the wire. By this shifting, selected bits can be addressed. Each of these operations is also discussed in some detail in section "Operation of Magnetic Domain Wall Devices" of this chapter, as these operations are the general ingredients for any domain wall-based device.

Apart from the prominent racetrack memory, other potential memory devices with domain walls exist. In Fig. 1b, a simplified 1-bit memory device is shown, and more recently, a 3D MRAM based on solitons in magnetic multilayers has been proposed [192]. Historically, already in the 1970s of the last century, magnetic bubble memory was a commercially available form of magnetic data storage. Therein, information is stored in the form of small magnetic bubble domains with opposite, out-of-plane magnetization with respect to an applied bias field, whose strength can be used to adjust the domain size. Bubbles are shifted by a rotating magnetic field along a guiding electrode structure at whose ends reading and writing is performed. Information is moved only in one sense of direction and in all lines in parallel; therefore, bits need to be read and rewritten all the time as they pass to the end of the electrode structure [193].

Field-Controlled Shift Register

While current-induced domain wall motion has raised huge interest, it is typically associated with huge current densities which are unfavorable for the stable operation of a device. A more conventional approach employs external magnetic fields for domain shifting. The immediate problem is that neighboring 180° domain walls (e.g., imagine one head-to-head and one tail-to-tail wall next to each other) will move in opposite directions under a strong enough magnetic field. Yet this problem can be overcome by using a kind of slip–stick motion as shown schematically in Fig. 21a–d. For this alternative [7, 194, 195], which was suggested by R. Cowburn, domain walls are selectively moved by a global field, the selectivity being realized by local variations of the pinning strength, e.g., through heating [7]. One cycle of movement consists of two opposite field pulses while activating neighboring pinning sites (notches) respectively.

Domain Wall Logic Devices

Logic devices using movable magnetic domain walls as information have been proposed, and the basic logical gates "and" and "not" have been successfully demonstrated in magnetic nanowires [196, 197]. The gates, as well as a fanning out device, were realized by combining planar joints/junctions of several nanowires of suitable geometry, i.e., in particularly adjusting the angle under which the wires

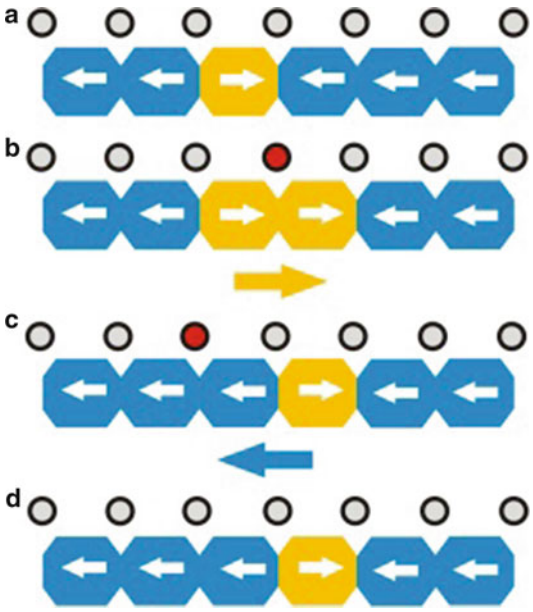

Fig. 21 Schematic of a shift register in which magnetic domains are moved by using thermally activated domain wall traps. The colors *yellow* and *blue* correspond to different magnetization directions. (**a**) A wire with periodically arranged notches exhibits different domain configurations between the traps. (**b**) By applying a field (*yellow arrow*) and heating one specific notch (*red dot*), the domain wall can be selectively depinned at this notch, enlarging one domain. (**c**) By heating a different notch and applying a field in the opposite direction (*blue arrow*), another domain wall is depinned and is caught at the next notch. (**d**) Thus, the whole domain is displaced one step forward compared to the initial state in (**a**), using this slip–stick motion [7] (From Ref. [126])

connect. Due to the nonvolatility of the magnetic systems, these logic devices combine logic and memory functionalities.

Nonvolatile Multiturn Sensors

Typical applications for magnetic domains and domain walls are, due to their digital nature, memory and logic. These examples, which have been mentioned above, are frequently discussed in the context of microelectronic and spintronic devices. However, devices based on magnetic domain walls can also be used in other areas, for instance, as sensors, as will be illustrated in this section. It will deal with two types of domain wall-based multiturn sensors, which are attractive for automotive and industrial application to successfully compete with existing mechanical turn or angle sensors. The first, spiral sensor with limited turns is already commercially available and may be used, for instance, to count, without

mechanical wear, the turns of a truck steering wheel. The second, closed loop sensor has a huge potential due to the high number of turns that can be counted, which together with a suitable leverage could result in cheap, high-precision angle sensors if current limitations of the magnetic working windows can be overcome.

These sensors combine the two aspects mentioned above, logic and memory, as they accomplish the counting and the storage of the number of half or full turns of a mechanical device. The big advantage of this sensor family is that the counting occurs powerless and wear-free, a property very attractive for many large-scale applications. The energy necessary for the creation/motion of a domain wall is spent by the acting magnetic field of, e.g., a rotating magnet, whose number of rotation has to be counted.

On the example of these devices, we will also try to examine some critical issues of domain wall devices. The purely magnetic nature of the writing and storing information in these multiturn sensors bears some clear advantages as no mechanical wear and nonvolatility. However, for the integration of the device, at some stage, the magnetic or spin signal needs to be read and converted into a charge signal for processing. In the present example a resistive readout is performed using the in-plane GMR effect of the magnetic stack. A resistive readout implies energy consumption and additional complexity and, thus, ultimately, cost. A fascinating, more advanced, and challenging option for any spintronic device would be the direct conversion of the spin signal into a logic state charge signal, and a direct spin current to charge current conversion can be obtained by the spin Hall effect.

Another critical issue of any device based on magnetic domain wall motion is the working window, which is limited on one side by the minimum stimulus (in this particular case the magnetic field, but it may be a current as well) needed to deterministically and reliably move the domain walls. On the other side, there is a maximum applicable stimulus before undesired transformations of the domain wall structure or nucleation of new domain walls occurs.

Multiturn Sensor Using the Generation and the Storage of 180° Domain Walls

The multiturn sensor based on a spiral geometry (Fig. 22) exploits the shape dependence of the remagnetization process for small structures to generate and move magnetic domain walls. Connecting a magnetic nanowire with a bigger magnetic pad, 180° domain walls can be generated by a magnetic field which is sufficient to invert the magnetization of the pad but not the one of the wire, which has an enhanced anisotropy field H_k due to its elongated shape. After the domain wall was generated, it can then be moved through the nanowire by a rotation of the magnetic field H_{rot} which is big enough to overcome the pinning of the domain wall [199].

A layout used in first industrial application of multiturn sensors [198, 200, 201] separates the individual 180° domain walls by introducing 90° bends in the nanowire, as shown in Fig. 22a schematically. A dark field micrograph of the chip is shown in Fig. 22b. The nanowire forms a spiral with N turns, made from a GMR stack. Starting with a single domain configuration, where the magnetization

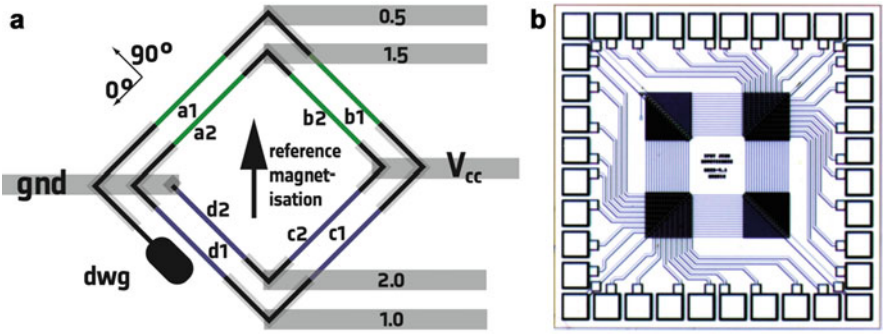

Fig. 22 (**a**) Schematic sketch of the sensor geometry for a 2-turn counter. The straight stripes of the spiral build four half bridges (Nanowires a1 + b1,a2 + b2, c1 + d1, and c2 + d2) for the detection of 0.5 turns and 1.5 turns (*green colored*) in the upper sensor part and for the detection of 1 turn and 2 turns (*blue colored*) in the lower sensor part. Read out by connecting contact (0.5 . . . 2.0) bridge voltage between gnd and V_{CC}. (**b**) Inverted dark field light microscope image of a $N = 16$ multiturn counter with simple circuiting. The die size is 1.1×1.1 mm^2, with a stripe length between the contacts of 200 µm. The innermost 17th turn is separated from the spiral and could be used for generation of a reference signal (From Ref. [198])

describes a continuous way through the spiral from the inner, tapered to the outer end in the shape of a large area with therefore small in-plane anisotropy, different magnetic states of a soft part of the GMR stack can be realized while keeping the magnetization of the reference layer fixed.

A first 180° rotation of the magnetic field in the sense of the spiral, here clockwise (cw), creates a 180° domain wall between the enlarged part called domain wall generator (DWG) and the nanowire and moves the domain wall inside this spiral. This step determines the lowest magnetic field usable in this geometry. The strength of the rotating magnetic field must be larger than the minimum field $H_{\min}$ necessary for a pinning-free movement of the domain wall through the spiral, i.e., $H_{\min} < H_{\rm rot} < H_{\max}$, whereas the largest field $H_{\max} \sim H_{\rm k}^{\rm nanowire}/2$ applicable is determined by the spiral itself, preventing unwanted domain wall generation. The second half turn in cw direction generates the second domain wall in the domain wall generator and moves it into the spiral. Synchronously the first domain wall moves an additional half turn within the spiral in the cw direction. This process can be repeated in a spiral with N turns until 2 N domain walls are stored, while every further cw rotation does not change the number of domain walls in the spiral because the domain wall sitting in the innermost turn reaches the tapered end, remagnetizes it, and vanishes in doing so.

For a counterclockwise (ccw) rotation by 180°, also a new domain wall will be created in the domain wall generator which moves into the spiral. If the spiral is at least partially filled from cw rotation, the domain walls already inside the spiral move a half turn in the ccw direction. The outermost moving domain wall meets the newly generated domain wall, and the two annihilate each other. Therefore, every

half turn in a direction antiparallel to the sense of the spiral decreases the number of domain wall by one until the spiral is empty. Proper mechanical design has to avoid both a further ccw rotation for an empty and a cw rotation for a full spiral.

The readout of the number of domain wall sitting in the spiral can be performed by a control of the half bridge voltages as shown in Fig. 22a. The half and full turn contacts named 0.5, 1.5, and 1.0, 2.0 form Wheatstone half bridges which allow the suppression of the influence of the temperature coefficient of the spiral itself. As long as the corner of the spiral between a*i* and b*i* contains a domain wall, the voltage level at this corner is equal to 0.5 V_{CC}. Otherwise the voltage is $(0.5 \pm 0.35 * \Delta R/R) * V_{CC}$ with $\Delta R/R$ the GMR effect of the stack. As discussed in more detail in [198], only either the half or the full turn pads give an unambiguous signal level due to the hysteretic nature of the movement of the domain walls through the wire. To select between both cases, the magnetization direction within the angle range (0–360°) has to be measured using an angle detector.

Universal Multiturn Sensor Based on Pure Domain Wall Movement

The limitation on the number of turns workable in a single N turn spiral can be overcome by the use of different closed loops which are loaded with a predefined constant number of domain walls, preferably one, per loop [202]. As shown in Fig. 23 and discussed in detail by Allwood et al. [196], the movement of one domain wall through a closed loop requires a 360° field rotation plus an additional 180° for each cusp of the loop. Thus the number of cusps M fixes the number of half turns N of the magnetic field needed to move a domain wall all around to its starting position to $N = (M + 2)/2$. The magnetization configuration of the loop is reversed after this one domain wall motion, and it needs another N half turns field rotation to end up with the starting configuration. It holds for every odd (here one) number of cusps that the starting configuration of the magnetization configuration is reached

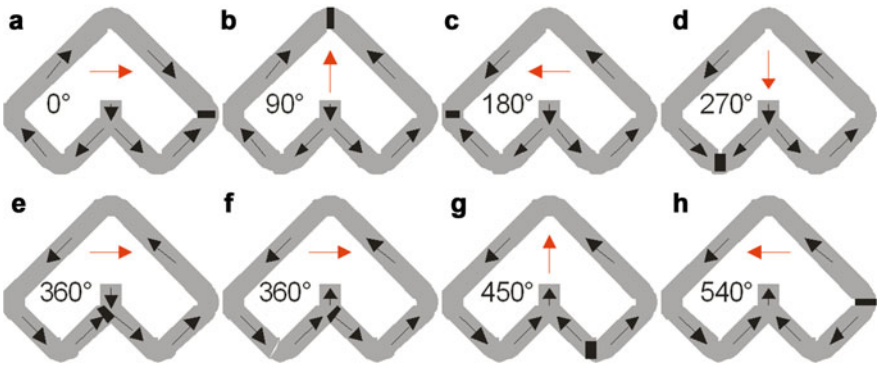

Fig. 23 Movement of a domain wall through a loop with one cusp for a rotating magnetic field (*red arrow*) in the ccw direction in steps of 90°. The magnetization state in the loop and the domain wall position are indicated by *black arrows* and a *black rectangular*, respectively. The field angle of the rotating external field is given as number and illustrated as *red arrow*

after (M + 2) full field rotations, i.e., for instance, a loop for counting 5 turns has 3 cusps. Combining loops with coprime numbers of turns, a total large number of turns can be uniquely identified, e.g., with 6 loops, a total of $5 \times 7 \times 9 \times 11 \times 13 \times 17 \times 19 = 14.55 * 10^6$ turns can be counted.

The readout of the individual loops can be performed by using the GMR or TMR effect. By forming a Wheatstone half bridge, the temperature coefficient of the resistance can be suppressed similarly as discussed above. As explained in Refs. [203, 204], a loop with M cusps requires M + 4 contact pads to fully characterize the position of the domain wall inside the loop. The total number of pads increases very slowly, approximately logarithmically, with the number of turns the combined sensor has to count, resulting in 100 contact pads for the example above of $14.55*10^6$ turns, while with only two more loops and a total of 156 contacts, already 10^{10} turns are reachable. The logarithmic increase in the electronic complexity shows the big potential of this sensor if large numbers of turns need to be counted. Also a pure forward or backward counter can be built by implementing a magnetic diode as described in [203, 204]. However, the magnetic working window will be modified because then the maximum field is additionally limited by the maximum working field of the magnetic diode avoiding a contrary domain wall movement.

The applicability of such sensors is determined by different aspects, e.g., the magnetic window the sensor needs to work at, the maximum speed the sensor can follow, the integration into the complete systems, and the die size, which also determines the sensor prize. The magnetic window is determined by the geometrical features of the sensing layer within the GMR stack, i.e., the layer carrying the domains. Here the thickness should not be larger than 40–50 nm to avoid too small GMR $\Delta R/R$ signals. The width should be as small as possible to get a huge H_k and therefore a large $H_{\max}$. The last parameter, the minimum field necessary for a definite domain wall motion, depends on the edge roughness and its relation to the width. The maximum angular velocity depends on the length of the straight parts of the sensor and the hysteresis and is in the order of 10^8–10^9 turns/s typically. The number of countable turns determines the size and the number of pads. For low turn numbers ($\leq$64), the number of pads does not exceed 32, allowing for a remarkable die size below 1 mm^2 and easy electronic processing. For large turn numbers, the die size will be between 1 and 2 mm^2 and requires enhanced electronic circuiting.

Conclusions

In summary, we have reviewed devices based on magnetic domain walls in nanowires. We have treated the key properties of domain walls in different material classes and assessed them for the use in a device. We first discussed the domain wall spin structures most commonly found in thin wires (this geometry is sometimes also called stripes). For in-plane magnetized soft materials, the complex domain wall

types occurring and the dependence of the spin structure on the wire geometry are presented, and the more conventional domain wall types in out-of-plane magnetized materials are discussed.

Then an overview over the status and progress in terms of controlling the basic operations nucleation, displacement, and detection on domain walls, which would correspond, e.g., writing, addressing, and reading bits of information in a memory device, is given. Particular examples of memory devices using magnetic domain walls are discussed. These include memory devices, where a number of domain walls are shifted synchronously by injection of current pulses along a vertically integrated wire, with each domain wall carrying one bit. Such devices potentially combine the high density and low cost of the hard disk approach with the reliability of solid-state memory, due to the absence of mechanically moving parts. A magnetic random access memory (MRAM) architecture has also been proposed where the magnetic bit is written by propagation of a domain wall in a narrow track and despite a more complex three terminal architecture compared with standard MRAM, a low writing current could be obtained even for relatively high current density due to the small cross-section area of the track. In addition, this design bypasses the reliability issue in spin-torque MRAM due to damage of the thin insulating barrier of the magnetic tunnel junction when injecting high current densities. Additionally logic and sensor devices are described, and here the nonvolatility of the magnetic domain walls automatically combines them with a memory, thus adding functionality.

The basic requirements for any device are narrow domain walls (ideally a few nm), and thus out-of-plane magnetized high-anisotropy materials, and in particular for memory devices a domain wall velocity on the order of 100 m/s to achieve not only competitive areal density but also high operating speed. Sufficiently low write and read currents are also needed to guarantee low power consumption and small addressing transistor as well as low current density to avoid damage due to electromigration and information losses due to the Joule heating.

While significant progress has been made in many of these fields and first devices (such as sensors) have made it into the market, still fundamental research is needed to make domain wall devices viable alternatives for memories and logic elements that can capture a significant market share.

Acknowledgments We thank F. Büttner, A. Bisig, and C. Moutafis for help with various parts of the text and I. Berber for her support. We thank D. Hinzke and U. Nowak for permission to use Fig. 16 and D. Ravelosona for permission to use Figs. 8 and 9.

The authors would like to acknowledge the financial support by the DFG (SFB 767, SPP Graphene, SPP SpinCaT, KL1811), the Landesstiftung Baden Württemberg, the European Research Council via its Starting Independent Researcher Grant (Grant No. ERC-2007-Stg 208162) and Proof-of-Concept Grant schemes, EU RTN SPINSWITCH (MRTN-CT2006035327), the EU IP project IFOX (NMP3-LA-2010 246102), the EU STREP project MAGWIRE (FP7-ICT-2009-5 257707), the EU STREP project MoQuas (FP7-ICT-2013-10 610449), the EU ITN WALL (FP7-PEOPLE-2013-ITN 608031), the Swiss National Science Foundation, and the Graduate School of Excellence Materials Science in Mainz (MAINZ – GSC 266).

References

1. McFadyen R, Fullerton EE, Carey MJ (2006) State-of-the-art magnetic hard disk drives. MRS Bull 31:379
2. Dee RH (2006) Magnetic tape: the challenge of reaching hard-disk-drive data densities on flexible media. MRS Bull 31:404
3. Boulle O, Malinowski G, Kläui M (2011) Current-induced domain wall motion in nanoscale ferromagnetic elements. Mater Sci Eng R72:159
4. Tehrani S, Slaughter JM, Chen E, Durlam M, Shi J, DeHerrera M (1999) Progress and outlook for MRAM technology. IEEE Trans Magn 35:2814
5. Parkin SSP (2004) Shiftable magnetic shift register and method of using the same. US Patent 6,834,005 and Parkin SSP (2006) Magnetic shift register with shiftable magnetic domains between two regions, and method of using the same. US Patent 7031178 B2
6. Parkin SSP, Hayashi M, Thomas L (2008) Magnetic domain-wall racetrack memory. Science 320:190
7. Cowburn R, Petit D, Read D, Petracic O (2007) Data storage device and method. Patent WO 2007/132174A1
8. Parkin SSP (2006) MRS Bull 31:389
9. Kläui M (2008) Head-to-head domain walls in magnetic nanostructures. J Phys Condens Matter 20:313001
10. Kläui M, Vaz CAF (2007) Magnetization configurations and reversal in small magnetic elements. In: Kronmüller H, Parkin SSP (eds) Handbook of magnetism and advanced magnetic materials, vol 2. Wiley, Chichester
11. Kronmüller H, Fähnle M (2003) Micromagnetism and the microstructure of ferromagnetic solids. Cambridge University Press, Cambridge
12. Rhensius J, Vaz CAF, Bisig A, Schweitzer S, Heidler J, Körner HS, Locatelli A, Niño MA, Weigand M, Méchin L, Gaucher F, Goering E, Heyderman LJ, Kläui M (2011) Control of spin configuration in half-metallic La0.7Sr0.3MnO3 nano-structures. Appl Phys Lett 99:062508
13. Fonin M, Hartung C, Rüdiger U, Backes D, Heyderman L, Nolting F, Fraile Rodríguez A, Kläui M (2011) Formation of magnetic domains and domain walls in epitaxial Fe_3O_4(100) elements (invited). J Appl Phys 109:07D315
14. Bruno P (1999) Geometrically constrained magnetic wall. Phys Rev Lett 83:2425
15. Jubert PO, Allenspach R, Bischof A (2004) Magnetic domain walls in constrained geometries. Phys Rev B 69:220410
16. Vaz CAF, Bland JAC, Lauhoff G (2008) Magnetism in ultrathin film structures. Rep Prog Phys 71:056501
17. Dennis CL et al (2002) The defining length scales of mesomagnetism: a review. J Phys Cond Mat 14:R1175
18. Parkin S, Yang SH (2015) Memory on the Ractrack, Nature Nanotech. 10:195
19. Thiaville A, Nakatani Y (2006) Domain-wall dynamics in nanowires and nanostrips. In: Hillebrands B, Ounadjela K (eds) Spin dynamics in confined magnetic structures, vol 3. Springer, Berlin
20. Miltat J, Donahue MJ (2007) Numerical micromagnetics: finite difference methods. In: Kronmüller H, Parkin SSP (eds) Handbook of magnetism and advanced magnetic materials, vol 2. Wiley, Chichester
21. Schrefl T et al. (2007) Numerical methods in micromagnetics (finite element method). In: Kronmüller H, Parkin SSP (eds) Handbook of magnetism and advanced magnetic materials, vol 2. Wiley, Chichester
22. McMichael RD, Donahue MJ (1997) Head to head domain wall structures in thin magnetic strips. IEEE Trans Magn 33:4167
23. Kläui M, Vaz CAF, Bland JAC, Heyderman LJ, Nolting F, Pavlovska A, Bauer E, Cherifi S, Heun S, Locatelli A (2004) Head-to-head domain wall phase diagram in mesoscopic ring magnets. Appl Phys Lett 85:5637

24. Laufenberg M et al (2006) Observation of thermally activated domain wall transformations. Appl Phys Lett 88:052507
25. Wachowiak A, Wiebe J, Bode M, Pietzsch O, Morgenstern M, Wiesendanger R (2002) Direct observation of internal spin structure of magnetic vortex cores. Science 298:577
26. Junginger F, Kläui M, Backes D, Krzyk S, Rüdiger U, Kasama T, Dunin-Borkowski RE, Feinberg JM, Harrison RJ, Heyderman LJ (2008) Quantitative determination of vortex core dimensions in head-to-head domain walls using off-axis electron holography. Appl Phys Lett 92:112502
27. Feldtkeller E, Thomas H (1965) Struktur und Energie von Blochlinien in dünnen ferromagnetischen Schichten. Phys Kondens Mater 4:8
28. Nakatani Y, Thiaville A, Miltat J (2005) Head-to-head domain walls in soft nano-strips: A refined phase diagram. J Magn Magn Mater 290:750
29. Backes D et al (2007) Transverse domain walls in nanoconstrictions. Appl Phys Lett 91:112502
30. The Object Oriented MicroMagnetic Framework project, ITL = NIST. For details see, http://math.nist.gov/oommf
31. Hashim I, Joo HS, Atwater HA (1995) Structural and magnetic properties of epitaxial $Ni_{80}Fe_{20}$ thin films on Cu/Si. Surf Rev Lett 2:427
32. Alexe M, Ziese M, Hesse D, Esquinazi P, Yamauchi K, Fukushima T, Picozzi S, Gösele U (2009) Ferroelectric switching in multiferroic magnetite (Fe_3O_4) thin films. Adv Mater 21:4452
33. Dedkov YS, Rüdiger U, Günterodt G (2002) Evidence for the half-metallic ferromagnetic state of Fe_3O_4 by spin-resolved photoelectron spectroscopy. Phys Rev B 65:064417
34. Fonin M, Pentcheva R, Dedkov YS, Sperlich M, Vyalikh DV, Scheffler M, Rüdiger U, Güntherodt G (2005) Surface electronic structure of the Fe3O4 (100): Evidence of a half-metal to metal transition. Phys Rev B 72:104436
35. Fonin M, Dedkov YS, Pentcheva R, Rüdiger U, Güntherodt G (2007) Magnetite: a search for the half-metallic state. J Phys Condens Matter 19:315217
36. Kläui M, Vaz CAF, Lopez-Diaz L, Bland JAC (2003) Vortex Formation in narrow ferromagnetic rings. J Phys Condens Matter 15:R985
37. Coey JMD, Viret M, von Molnár S (1999) Mixed-valence manganites. Adv Phys 48:167
38. Dagotto E (2005) Complexity in strongly correlated electronic systems. Science 309:257
39. Wohlhüter P et al (2013) The effect of magnetic anisotropy on the spin configurations of patterned $La_{0.7}Sr_{0.3}MnO_3$ elements. J Phys Condens Matter 25:176004
40. Arnal T, Khvalkovskii AV, Bibes M, Mercey B, Lecoeur P, Haghiri-Gosnet A-M (2007) Electronic properties of domain walls in $La_{2/3}Sr_{1/3}MnO_3$: Magnetotransport measurements on a nanopatterned device. Phys Rev B75:220409R
41. Ruotolo A, Oropallo A, Miletto Granozio F, Pepe GP, Perna P, Scottidi Uccio U, Pullini D (2007) Current-induced domain wall depinning and magnetoresistance in La0.7Sr0.3MnO3 planar spin-valves. Appl Phys Lett 91:132502
42. Foerster M et al (2014) Efficient spin transfer torque in La2/3Sr1/3MnO3 nanostructures. Appl Phys Lett 104:072410
43. Finizio S et al (2014) Domain wall transformations and hopping in $La0.7Sr0.3MnO_3$ nanostructures imaged with high resolution x-ray magnetic microscopy. J Phys Cond Matter 26:456003
44. Jourdan M, Minar J, Braun J, Kronenberg A, Chadov S, Balke B, Gloskovskii A, Kolbe M, Elmers HJ, Schönhense G, Ebert H, Felser C, Kläui M (2014) Direct observation of half-metallicity in the Heusler compound Co2MnSi. Nat Commun 5:3974
45. Vaz AF, Rhensius J, Heidler J, Wohlhüter P, Bisig A, Körner HS, Mentes TO, Locatelli A, Le Guyader L, Nolting F, Graf T, Felser C, Heyderman LJ, Kläui M (2011) Spin configurations in Co(2)FeAl(0.4)Si(0.6) Heusler alloy thin film elements. Appl Phys Lett 99:182510

46. Miyawaki T et al. (2013) The effect of magnetocrystalline anisotropy on the domain structure of patterned Fe2CrSi Heusler alloy thin films. J Appl Phys 114:073905
47. Kläui M et al (2005) Appl Phys Lett 87:102509
48. Rothman J, Kläui M, Lopez-Diaz L, Vaz CAF, Bleloch A, Bland JAC, Cui Z, Speaks R (2001) Observation of a bi-domain state and nucleation free switching in mesoscopic ring magnets. Phys Rev Lett 86:1098
49. Harte KJ (1968) Theory of magnetization ripple in ferromagnetic films. J Appl Phys 39:1503
50. Kläui M, Jubert PO, Allenspach R, Bischof A, Bland JAC, Faini G, Rüdiger U, Vaz CAF, Vila L, Vouille C (2005) Direct observation of domain-wall configurations transformed by spin currents. Phys Rev Lett 95:026601
51. Hayashi M, Thomas L, Bazaliy YB, Rettner C, Moriya R, Jiang X, Parkin SSP (2006) Influence of current on field-driven domain wall motion in permalloy nanowires from time resolved measurements of anisotropic magnetoresistance. Phys Rev Lett 96:197207
52. Togawa Y, Kimura T, Harada K, Matsuda T, Tonomura A, Otani Y, Akashi T (2008) Current-excited magnetization reversal under in-plane magnetic field in a nanoscaled ferromagnetic wire. Appl Phys Lett 92:012505
53. Hubert A, Schäfer R (1998) Magnetic domains. Springer, Berlin
54. Sobolev VL (1998) Internal structure of a domain wall in ultrathin magnetic film. J Magn Magn Mater 177:195
55. Boulle O et al (2009) Reversible switching between bidomain states by injection of current pulses in a magnetic wire with out-of-plane magnetization. J Appl Phys 105:07C106
56. Mougin A, Cormier M, Adam JP, Metaxas PJ, Ferre J (2007) Domain wall mobility, stability and Walker breakdown in magnetic nanowires. Europhys Lett 78:57007
57. Ueda K et al. (2011) Current-induced domain wall motion in Co/Ni nano-wires with different Co and Ni thicknesses. J Phys Conf Ser 266:012110
58. Ohshima N et al. (2011) Real space observation of current-induced magnetic domain wall displacement in Co/Ni nano-wire by photoemission electron microscopy. J Phys Condens Matter 23:382202
59. Chiba D et al. (2010) Control of multiple magnetic domain walls by current in a Co/Ni nanowire. Appl Phys Expr 3:073004
60. O'Brien L, Petit D, Zeng HT, Lewis ER, Sampaio J, Jausovec AV, Read DE, Cowburn RP (2009) Near-field interaction between domain walls in adjacent permalloy nanowires. Phys Rev Lett 103:077206
61. Ahn SM, Moon KW, Cho CG, Choe SB (2011) Control of domain wall pinning in ferromagnetic nanowires by magnetic stray fields. Nanotechnology 22:085201
62. Kuch W, Chelaru LI, Fukumoto K, Porrati F, Offi F, Kotsugi M, Kirschner J (2003) Layer-resolved imaging of magnetic interlayer coupling by domain-wall stray fields. Phys Rev B 67:214403
63. Yang S.-H. et al. (2015) Domain-wall velocities of up to 750 m s^{-1} driven by exchange-coupling torque in synthetic antiferromagnets Nature Nanotech 10:221
64. Katine JA, Albert FJ, Buhrman RA, Myers EB, Ralph DC (2000) Current-driven magnetization reversal and spin-wave excitations in Co/Cu/Co pillars. Phys Rev Lett 84:3149
65. Lee OJ et al (2009) Ultrafast switching of a nanomagnet by a combined out-of-plane and in-plane polarized spin current pulse. Appl Phys Lett 95:012506
66. Papusoi C, Delaet B, Rodmacq B, Houssameddine D, Michel JP, Ebels U, Sousa RC, Buda-Prejbeanu L, Dieny B (2009) 100 ps precessional spin-transfer switching of a planar magnetic random access memory cell with perpendicular spin polarizer. Appl Phys Lett 95:072506
67. Liu H, Bedau D, Backes D, Kantine JA, Langer J, Kent AD (2010) Ultrafast switching in magnetic tunnel junction based orthogonal spin transfer devices. Appl Phys Lett 97:242510
68. Rowlands GE et al (2011) Ultrafast switching in magnetic tunnel junction based orthogonal spin transfer devices. Appl Phys Lett 98:102509
69. Amiri H et al (2011) Ultrafast switching in magnetic tunnel junction based orthogonal spin transfer devices. Appl Phys Lett 98:112507

70. Ikeda S, Miura K, Yamamoto H, Mizunuma K, Gan HD, Endo M, Kanai S, Hayakawa J, Matsukura F, Ohno H (2010) A perpendicular-anisotropy CoFeB–MgO magnetic tunnel junction. Nat Mater 9:721
71. Kammerer M et al (2011) Magnetic vortex core reversal by excitation of spin waves. Nat Comm 2:279
72. Landau L, Lifshits E (1935) On the theory of the dispersion of magnetic permeability in ferromagnetic bodies. Physikalische Zeitschrift der Sowjetunion 8:153
73. Brown WF (1963) Micromagnetics. Interscience, New York
74. Gilbert TL (2004) A phenomenological theory of damping in ferromagnetic materials. IEEE Trans Magn 40:3443
75. Thiaville A, Nakatani Y, Miltat J, Suzuki Y (2005) Micromagnetic understanding of current-driven domain wall motion in patterned nanowires. Europhys Lett 69:990
76. Tatara G, Kohno H (2004) Theory of current-driven domain wall motion: spin transfer versus momentum transfer. Phys Rev Lett 92:086601
77. Zhang S, Li Z (2004) Roles of nonequilibrium conduction electrons on the magnetization dynamics of ferromagnets. Phys Rev Lett 93:127204
78. Tatara G (2007) Spin torque and force due to current for general spin textures. J Phys Soc Japan 76:54707
79. Barnes SE, Maekawa S. Theory of spin-transfer torque and domain wall motion in magnetic nanostructures. In: Maekawa S (ed) Concepts in spin electronics. Oxford University Press, Oxford
80. Tserkovnyak Y, Brataas A, Bauer GEW (2008) Theory of current-driven magnetization dynamics in inhomogeneous ferromagnets. J Magn Magn Mater 320:1282
81. Schryer NL, Walker LR (1974) The motion of 180° domain walls in uniform dc magnetic fields. J Appl Phys 45:5406
82. Schieback C, Kläui M, Nowak U, Rüdiger U, Nielaba P (2007) Numerical investigation of spin-torque using the Heisenberg model. Eur Phys J B 59:429
83. Bryan MT, Schrefl T, Atkinson D, Allwood DA (2008) Magnetic domain wall propagation in nanowires under transverse magnetic fields. J Appl Phys 103:073906
84. Bryan MT, Schrefl T, Allwood DA (2010) Dependence of transverse domain wall dynamics on permalloy nanowire dimensions. IEEE Trans Magn 46:1135
85. Choi YS, Lee JY, Yoo MW, Lee KS, Guslienko KY, Kim SK (2009) Critical nucleation size of vortex core for domain wall transformation in soft magnetic thin film nanostrips. Phys Rev B 80:012402
86. Dean JS, Bryan MT, Allwood DA, Bance S, Bashir MA, Hrkac G (2009) Tailoring domain wall dynamics with uniaxial anisotropy in nanowires. IEEE Trans Magn 45:4067
87. Kim SK, Lee JY, Choi YS, Guslienko KY, Lee KS (2008) Underlying mechanism of domain-wall motions in soft magnetic thin-film nanostripes beyond the velocity breakdown regime. Appl Phys Lett 93:052503
88. Kunz A, Reiff SC (2008) Enhancing domain wall speed in nanowires with transverse magnetic fields. J Appl Phys 103:07D903
89. Breitbach E, Smith C, Kunz AJ (2009) Anti-vortex dynamics in magnetic nanostripes. J Appl Phys 103:07D502
90. Kunz A (2006) Simulating the maximum domain wall speed in a magnetic nanowire. IEEE Trans Magn 42:3219–3221
91. Kunz A (2006) Simulated domain wall dynamics in permalloy nanowires. J Appl Phys 99**:**08G107
92. Lee JY et al (2007) Dynamic transformations of the internal structure of a moving domain wall in magnetic nanostripes. Phys Rev B 76:184408
93. Martinez E, Lopez-Diaz L, Torres L, Tristan C, Alejos O (2007) Thermal effects in domain wall motion: Micromagnetic simulations and analytical model. Phys Rev B 75:174409
94. Nakatani Y, Thiaville A, Miltat J (2003) Faster magnetic walls in rough wires. Nat Mater 2:521

95. Zeisberger M, Mattheis R (2012) Magnetization reversal in magnetic nanostripes via Bloch wall formation. J Phys Condens Matter 24:024202
96. Berkov DV, Gorn NL MicroMagus: package for micromagnetic simulations. http://www.micromagus.de
97. Lu J, Wang XR (2010) Motion of transverse domain walls in thin magnetic nanostripes under transverse magnetic fields. J Appl Phys 107:083915
98. Ono T, Miyajima H, Shigeto K, Shinjo T (1998) Magnetization reversal in sub-micron magnetic wire studied by using giant magnetoresistance effect. Appl Phys Lett 72:1116
99. Ono T, Miyajima H, Shigeto K, Mibu K, Hosoito N, Shinjo T (1999) Propagation of a magnetic domain wall in a submicrometer magnetic wire. Science 284:468
100. Atkinson D, Allwood DA, Xiong G, Cooke MD, Faulkner CC, Cowburn RP (2003) Magnetic domain-wall dynamics in a submicrometre ferromagnetic structure. Nat Mater 2:85
101. Beach GSD, Nistor C, Knutson C, Tsoi M, Erskine JL (2005) Dynamics of field-driven domain-wall propagation in ferromagnetic nanowires. Nat Mater 4:741
102. Yang J, Nistor C, Beach GSD, Erskine JL (2008) Magnetic domain-wall velocity oscillations in permalloy nanowires. Phys Rev B 77:014413
103. Hayashi M, Thomas L, Rettner C, Moriya R, Parkin SSP (2007) Direct observation of the coherent precession of magnetic domain walls propagating along permalloy nanowires. Nat Phys 3:21
104. Hayashi M, Thomas L, Rettner C, Moriya R, Parkin SSP (2008) Real time observation of the field driven periodic transformation of domain walls in Permalloy nanowires at the Larmor frequency and its first harmonic. Appl Phys Lett 92:112510
105. Glathe S, Mattheis R, Berkov DV (2008) Direct observation and control of the Walker breakdown process during a field driven domain wall motion. Appl Phys Lett 93:072508
106. Glathe S, Berkov I, Mikolajick T, Mattheis R (2008) Experimental study of domain wall motion in long nanostrips under the influence of a transverse field. Appl Phys Lett 93:162505
107. Weerts K, Van Roy W, Borghs G, Lagae L (2010) Suppression of complex domain wall behaviour in Ni80Fe20 nanowires by oscillating magnetic fields. Appl Phys Lett 96:062502
108. Lewis ER, Petit D, O'Brien L, Fernandez-Pacheco A, Sampaio J, Jausovec AV, Zeng HT, Read DE, Cowburn RP (2010) Fast domain wall motion in magnetic comb structures. Nat Mater 9:980
109. Glathe S, Zeisberger M, Hübner U, Mattheis R, Berkov DV (2010) Splitting of a moving transverse domain wall in a magnetic nanostripe in a transverse field. Phys Rev B 81:020412(R)
110. Zinoni C, Vanhaverbeke A, Eib P, Salis G, Allenspach R (2011) Beyond the compact magnetic domain wall. Phys Rev Lett 107:207204
111. Hayashi M, Kasai S, Mitani S (2010) Time resolved inductive detection of domain wall dynamics in magnetic nanowires. App Phys Express 3:113004
112. Moriya R, Hayashi M, Thomas L, Rettner C, Parkin SSP (2010) Dependence of field driven domain wall velocity on cross-sectional area in Ni65Fe20Co15 nanowire. Appl Phys Lett 97:142506
113. Jiang X, Thomas L, Moriya R, Hayashi M, Bergman B, Rettner C, Parkin SSP (2010) Enhanced stochasticity of domain wall motion in magnetic racetracks due to dynamic pinning. Nat Commun 1:25
114. Kondou K, Ohshima N, Kasai S, Nakatani Y, Ono T (2008) Single shot detection of the magnetic domain wall motion by using tunnel magnetoresistance effect. Appl Phys Express 1:061302
115. Rhensius J, Heyne L, Backes D, Krzyk S, Heyderman LJ, Joly L, Nolting F, Kläui M (2010) Imaging of domain wall inertia in permalloy half-ring nanowires by time-resolved photoemission electron microscopy. Phys Rev Lett 104:067201
116. Kim J-S, Kläui M (2014) Magnetic device switchable by magnetic domain wall motion and method of operating the device. Patent EP2747086 A1
117. Seo S M et al. (2007) Effect of shape anisotropy on threshold current density for current-induced domain wall motion. Appl Phys Lett 90:252508

118. Yamaguchi A, Ono T, Nasu S, Miyake K, Mibu K, Shinjo T (2004) Real-space observation of current-driven domain wall motion in submicron magnetic wires. Phys Rev Lett 92:077205
119. Kläui M, Vaz CAF, Bland JAC, Wernsdorfer W, Faini G, Cambril E, Heyderman LJ, Nolting F, Rüdiger U (2005) Controlled and reproducible domain wall displacement by current pulses injected into ferromagnetic ring structures. Phys Rev Lett 94:106601
120. Meier G et al (2007) Direct imaging of stochastic domain-wall motion driven by nanosecond current pulses. Phys Rev Lett 98:187202
121. Marrows H (2005) Spin-polarised currents and magnetic domain walls. Adv Phys 54:585
122. Beach GSD, Knutson C, Nistor C, Tsoi M, Erskine JL (2007) Nonlinear domain-wall velocity enhancement by spin-polarized electric current. Phys Rev Lett 97:057203
123. Hayashi M, Thomas L, Rettner C, Moriya R, Bazaliy YB, Parkin SSP (2007) Current driven domain wall velocities exceeding the spin angular momentum transfer rate in permalloy nanowires. Phys Rev Lett 98:037204
124. Jubert PO, Kläui M, Bischof A, Rüdiger U, Allenspach R (2006) Velocity of vortex walls moved by current. J Appl Phys 99:08G523
125. Heyne L et al (2008) Relationship between nonadiabaticity and damping in permalloy studied by current induced spin structure transformations. Phys Rev Lett 100:066603
126. Kläui M et al (2009) Concepts for domain wall motion in nanoscale ferromagnetic elements due to spin torque and in particular oersted fields. J Magn 14(2):53
127. Fukami S, Suzuki T, Ohshima N, Nagahara K, Ishiwata N (2008) Intrinsic threshold current density of domain wall motion in nanostrips with perpendicular magnetic anisotropy for use in low-write-current mrams. IEEE Trans Magn 44:2539
128. Suzuki T, Fukami S, Ohshima N, Nagahara K, Ishiwata N (2008) Analysis of current-driven domain wall motion from pinning sites in nanostrips with perpendicular magnetic anisotropy. J Appl Phys 103:113913
129. Fukami S, Suzuki T, Ohshima N, Nagahara K, Ishiwata N (2008) Micromagnetic analysis of current driven domain wall motion in nanostrips with perpendicular magnetic anisotropy. J Appl Phys 103:07E718
130. Fukami S, Nakatani Y, Suzuki T, Nagahara K, Ohshima N, Ishiwata N (2009) Relation between critical current of domain wall motion and wire dimension in perpendicularly magnetized Co/Ni nanowires. Appl Phys Lett 95:232504
131. Martinez E, Lopez-Diaz L, Alejos O, Torres L (2009) Thermally activated domain wall depinning in thin strips with high perpendicular magnetocrystalline anisotropy. J Appl Phys 106:043914
132. Garcia-Sanchez F, Szambolics H, Mihai AP, Vila L, Marty A, Attan JP, Toussaint JC, Buda-Prejbeanu LD (2010) Effect of crystalline defects on domain wall motion under field and current in nanowires with perpendicular magnetization. Phys Rev B 81:134408
133. Yan M, Kokay A, Gliga S, Hertel R (2010) Beating the walker limit with massless domain walls in cylindrical nanowires. Phys Rev Lett 104:057201
134. Tatara G, Entel P (2008) Calculation of current-induced torque from spin continuity equation. Phys Rev B 78:064429
135. Garate I, Gilmore K, Stiles MD, MacDonald AH (2009) Nonadiabatic spin-transfer torque in real materials. Phys Rev B 79:104416
136. Obata K, Tatara G (2008) Current-induced domain wall motion in Rashba spin-orbit system. Phys Rev B 77:214429
137. Lucassen ME, van Driel HJ, Morais Smith C, Duine RA (2009) Current-driven and field-driven domain walls at nonzero temperature. Phys Rev B 79:224411
138. Heinen J et al (2012) Determination of the spin torque non-adiabaticity in perpendicularly magnetized nanowires. J Phys Condens Matter 24:024220
139. Ravelosona D, Mangin S, Katine JA, Fullerton E, Terris BD (2007) Treshhold currents to move domain walls in film with perpendicular anisotropy. Appl Phys Lett 90:072508

140. Li S, Nakamura H, Kanazawa T, Liu X, Morisako A (2010) Current-Induced domain wall motion in TbFeCo wires with perpendicular magnetic anisotropy. IEEE Trans Magn 46:1695
141. Koyama T et al (2011) Observation of the intrinsic pinning of a magnetic domain wall in a ferromagnetic nanowire. Nat Mater 10:194
142. Suzuki T, Fukami S, Nagahara K, Ohshima N, Ishiwata N (2009) Evaluation of scalability for current-driven domain wall motion in a co/ni multilayer strip for memory applications. IEEE Trans Magn 45:3776
143. Tanigawa H, Koyama T, Yamada G, Chiba D, Kasai S, Fukami S, Suzuki T, Ohshima N, Ishiwata N, Nakatani Y, Ono T (2009) Domain wall motion induced by electric current in a perpendicularly magnetized Co/Ni nano-wire. Appl Phys Express 2:053002
144. Fukami S, Suzuki T, Nakatani Y, Ishiwata N, Yamanouchi M, Ikeda S, Kasai N, Ohno H (2011) Current-induced domain wall motion in perpendicularly magnetized CoFeB nanowire. Appl Phys Lett 98:082504
145. Lee JC, Kim KJ, Ryu J, Moon KW, Yun SJ, Gim GH, Lee KS, Shin KH, Lee HW, Choe SB (2011) Universality classes of magnetic domain wall motion. Phys Rev Lett 107:067201
146. Koyama T, Yamada G, Tanigawa H, Kasai S, Ohshima N, Fukami S, Ishiwata N, Nakatani Y, Ono T (2008) Control of domain wall position by electrical current in structured Co/Ni wire with perpendicular magnetic anisotropy. Appl Phys Express 1:101303
147. Moore TA, Miron IM, Gaudin G, Serret G, Auffret S, Rodmacq B, Schuhl A, Pizzini S, Vogel J, Bonfim M (2008) High domain wall velocities induced by current in ultrathin Pt/Co/AlOx wires with perpendicular magnetic anisotropy. Appl Phys Lett 93:262504
148. Miron M (2009) Etude de l'interaction entre un courant polarisé en spin et une paroi de domaine magnétique dans des matériaux à aimantation perpendiculaire. PhD thesis, Université Joseph Fourier
149. Miron M, Moore T, Szambolics H, Buda-Prejbeanu LD, Auffret S, Rodmacq B, Pizzini S, Vogel J, Bonfim M, Schuhl A, Gaudin G (2011) Fast current-induced domain-wall motion controlled by the Rashba effect. Nat Mater 10:419
150. Koyama T, Chiba D, Ueda K, Tanigawa H, Fukami S, Suzuki T, Ohshima N, Ishiwata N, Nakatani Y, Ono T (2011) Magnetic field insensitivity of magnetic domain wall velocity induced by electrical current in Co/Ni nanowire. Appl Phys Lett 98:192509
151. Miron M, Gaudin G, Auffret S, Rodmacq B, Schuhl A, Pizzini S, Vogel J, Gambardella P (2010) Current-driven spin torque induced by the Rashba effect in a ferromagnetic metal layer. Nat Mater 9:230
152. Ngo DT, Ikeda K, Awano H (2011) Direct observation of domain wall motion induced by low-current density in tbfeco wires. Appl Phys Express 4:093002
153. Miron M, Garello K, Gaudin G, Zermatten P, Costache MV, Auffret S, Bandiera S, Rodmacq B, Schuhl A, Gambardella P (2011) Perpendicular switching of a single ferromagnetic layer induced by in-plane current injection. Nature 476:189
154. Kim K, Seo S, Ryu J, Lee K, Lee H (2012) Magnetization dynamics induced by in-plane currents in ultrathin magnetic nanostructures with Rashba spin-orbit coupling. Phys Rev B 85:180404
155. Liu H, Pai CF, Li Y, Tseng HW, Ralph DC, Buhrman RA (2012) Spin-torque switching with the giant spin hall effect of tantalum. Science 336:555
156. Ryu K-S, Thomas L, Yang S-H, Parkin SSP (2013) Chiral spin torque at magnetic domain walls. Nat Nanotech 8:527
157. Emori S, Bauer U, Ahn S-M, Martinez E, Beach GSD (2013) Current-driven dynamics of chiral ferromagnetic domain walls. Nat Mater 12:611
158. Lo Conte R, Hrabec A, Mihai AP, Schulz T, Noh S-J, Marrows CH, Moore TA, Kläui M (2014) Spin-orbit torque-driven magnetization switching and thermal effects studied in Ta/CoFeB/MgO nanowires. Appl Phys Lett 105:122404
159. Lo Conte R et al (2015) Role of B diffusion in the interfacial Dzyaloshinskii-Moriya interaction in Ta/Co20Fe60B20/MgO nanowires. Phys Rev B 91:014433

160. Haney PM, Lee H-W, Lee K-J, Stiles MD (2013) Current induced torques and interfacial spin-orbit coupling: Semiclassical modeling. Phys Rev B 87:174411
161. Lee JY, Lee KS, Kim SK (2007) Remarkable enhancement of domain-wall velocity in magnetic nanostripes. Appl Phys Lett 91:122513
162. Vanhaverbeke A, Bischof A, Allenspach R (2008) Control of domain wall polarity by current pulses. Phys Rev Lett 101:107202
163. Rebei A, Mryasov O (2006) Dynamics of a trapped domain wall in a spin-valve nanostructure with current perpendicular to the plane. Phys Rev B. 74:014412
164. Khvalkovskiy V, Zvezdin KA, Gorbunov YV, Cros V, Grollier J, Fert A, Zvezdin AK (2009) High domain wall velocities due to spin currents perpendicular to the plane. Phys Rev Lett 102:067206
165. Boone CT, Katine JA, Carey M, Childress JR, Cheng X, Krivorotov IN (2010) Rapid domain wall motion in permalloy nanowires excited by a spin-polarized current applied perpendicular to the nanowire. Phys Rev Lett 104:097203
166. Boone CT, Krivorotov IN (2010) Magnetic domain wall pumping by spin transfer torque. Phys Rev Lett 104:167205
167. Chanthbouala A et al (2011) Vertical-current-induced domain-wall motion in MgO-based magnetic tunnel junctions with low current densities. Nat Phys **7**:626
168. Lavrijsen R, Malinowski G, Franken JH, Kohlhepp JT, Swagten HJM, Koopmans B, Czapkiewicz M, Stobiecki T (2010) Reduced domain wall pinning in ultrathin Pt/Co100-xBx/Pt with perpendicular magnetic anisotropy. Appl Phys Lett 96:022501
169. Gottwald M, Girod S, Andrieu S, Mangin S (2010) Tuneable perpendicular magnetic anisotropy in single crystal [Co/Ni](111) superlattices. IOP Conf Ser Mater Sci Eng 12:012018
170. Hinzke D, Nowak U (2011) Domain wall motion by the magnonic spin seebeck effect. Phys Rev Lett 107:027205
171. Franken JH, Möhrke P, Kläui M, Rhensius J, Heyderman LJ, Thiele J-U, Swagten HJM, Gibson UJ, Rüdiger U (2009) Effects of combined current injection and laser irradiation on Permalloy microwire switching. Appl Phys Lett 95:212502
172. Möhrke P, Rhensius J, Thiele JU, Heyderman LJ, Kläui M (2010) Tailoring laser-induced domain wall pinning. Solid State Commun 150:489
173. Uchida K, Takahashi S, Ieda J, Harii K, Ikeda K, Koshibae W, Maekawa S, Saitoh E (2009) Phenomenological analysis for spin-seebeck effect in metallic magnets. J Appl Phys 105:07C908
174. Jiang W et al (2013) Direct imaging of thermally driven domain wall motion in magnetic insulators. Phys Rev Lett 110:177202
175. You Y (2008) Another method for domain wall movement by a nonuniform transverse magnetic field. Appl Phys Lett 92:152507
176. You Y (2008) Equation of motion for a domain wall movement under a nonuniform transverse magnetic field. Appl Phys Lett 92:192514
177. Johnson M, Silsbee RH (1985) Equation of motion for a domain wall movement under a nonuniform transverse magnetic field. Phys Rev Lett 55:1790
178. Kimura T, Otani Y, Hamrle J (2006) Switching magnetization of a nanoscale ferromagnetic particle using nonlocal spin injection. Phys Rev Lett 96:037201
179. Jedema FJ, Filip AT, van Wees B (2001) Electrical spin injection and accumulation at room temperature in an all-metal mesoscopic spin valve. Nature 410:345
180. Ji Y, Hoffmann A, Jiang JS, Pearson JE, Bader SD (2007) Non-local spin injection in lateral spin valves. J Phys D Appl Phys 40:1280
181. Yang T, Kimura T, Laloe J-B, Otani Y (2008) Giant spin-accumulation signal and pure spin-current-induced reversible magnetization switching. Nat Phys 4:851
182. Kimura T, Otani Y (2007) Domain wall nucleation assisted by nonlocal spin injection. J Phys D Appl Phys 40:1285

183. Ilgaz D et al (2010) Domain-wall depinning assisted by pure spin currents. Phys Rev Lett 105:076601
184. Tombros N, Jozsa C, Popinciuc M, Jonkman HT, van Wees B (2007) Electronic spin transport and spin precession in single graphene layers at room temperature. Nature 448:571
185. Han D-S, Kim S-K, Lee J-Y, Hermsoerfer SJ, Schutheiss H, Leven B, Hillebrands B (2009) Magnetic domain-wall motion by propagating spin waves. Appl Phys Lett 94:112502
186. Jamali M, Yang H, Lee K-J (2010) Spin wave assisted current induced magnetic domain wall motion. Appl Phys Lett 96:242501
187. Kim JS, Stärk M, Kläui M, Yoon J, You CY, Lopez-Diaz L, Martinez E (2012) Interaction between propagating spin waves and domain walls on a ferromagnetic nanowire. Phys Rev B 85:174428
188. Kimel V, Kirilyuk A, Usachev PA, Pisarev RV, Balbashow AM, Rasing T (2005) Ultrafast non-thermal control of magnetization by instantaneous photomagnetic pulses. Nature 435:655
189. Bryan MT, Dean J, Allwood DA (2012) Dynamics of stress-induced domain wall motion. Phys Rev B 85:144411
190. Hockel JL, Bur A, Wu T, Wetzlar KP, Carman GP (2012) Electric field induced magnetization rotation in patterned Ni ring/$Pb(Mg_{1/3}Nb_{2/3})O_3](_{1–0.32})$-$[PbTiO3]_{0.32}$ heterostructures. Appl Phys Lett 100:022401
191. Finizio S et al (2014) Magnetic anisotropy engineering in thin film ni nanostructures by magnetoelastic coupling. Phys Rev Appl 1:021001
192. Lavrijsen R, Lee J-H, Fernandez-Pacheco A, Petit DC, Mansell R, Cowburn RP (2013) Magnetic ratchet for three-dimensional spintronic memory and logic. Nature 493:647
193. Malozemoff P, Slonczewski JC (1979) Magnetic domain walls in bubble materials. Academic, New York
194. Ilgaz D, Kläui M, Heyne L, Boulle O, Zinser F, Krzyk S, Fonin M, Rüdiger U, Backes D, Heyderman LJ (2008) Selective domain wall depinning by localized Oersted fields and Joule heating. Appl Phys Lett 93:132503
195. Ha S-S, You C-Y (2007) Validity of the analytic expression for the temperature of Joule heated nano-wire. J Magn 12:7
196. Allwood DA, Gang X, Cooke MD, Faulkner CC, Atkinson D, Vernier N, Cowburn RP (2002) Submicrometer ferromagnetic not gate and shift register. Science 296:2003
197. Allwood DA, Xiong G, Faulkner CC, Atkinson D, Petit D, Cowburn RP (2005) Magnetic domain-wall logic. Science 309:1688
198. Diegel M, Glathe S, Mattheis R, Scherzinger M, Halder E (2009) A new four bit magnetic domain wall based multiturn counter. IEEE Trans Magn 45:3792
199. Diegel M, Mattheis R, Halder E (2004) 360° Domain wall investigation for sensor applications. IEEE Trans Magn 40:2655
200. Diegel M, Mattheis R, Halder E (2007) Multiturn counter using movement and storage of 180° magnetic domain walls. Sensor Lett 5:118
201. The Novotechnik RSM 2800 sensor on www.novotechnik.de/en/products/rotary-sensors/
202. Mattheis R, Glathe S, Diegel M, Huebner U (2012) Concepts and steps for the realization of a new domain wall based GMR nanowire device: from the available 2^4 multiturn counter to a 2^{12} turn counter. J Appl Phys 111:113920
203. Allwood A, Gang X, Cowburn RP (2004) Domain wall diodes in ferromagnetic planar nanowires. Appl Phys Lett 85:2848
204. Bryan MT, Schrefl T, Allwood DA (2007) Symmetric and asymmetric domain wall diodes in magnetic nanowires. Appl Phys Lett 91:142502